Stem Cell Reports
Report
ISSCR
OPEN ACCESS

Synthetic augmentation of bilirubin metabolism in human pluripotent stem cell-derived liver organoids

Hasan Al Reza,[1,2] Zishaan Farooqui,[3] Abid Al Reza,[1] Callen Conroy,[4] Kentaro Iwasawa,[3] Yasuhiro Ogura,[5] Keisuke Okita,[6] Kenji Osafune,[6] and Takanori Takebe[1,2,3,7,8,9,*]

[1]Division of Developmental Biology, Cincinnati Children's Hospital Medical Center, Cincinnati, OH, USA
[2]Center for Stem Cell and Organoid Medicine (CuSTOM), Cincinnati Children's Hospital Medical Center, Cincinnati, OH, USA
[3]Division of Gastroenterology, Hepatology & Nutrition, Cincinnati Children's Hospital Medical Center, Cincinnati, OH, USA
[4]College of Medicine, University of Kentucky, Lexington, KY, USA
[5]Department of Transplantation Surgery, Nagoya University Hospital, Nagoya University Graduate School of Medicine, Aichi, Japan
[6]Center for iPS Cell Research and Application (CiRA), Kyoto University, Kyoto, Japan
[7]Institute of Research, Tokyo Medical and Dental University, Tokyo, Japan
[8]Department of Pediatrics, University of Cincinnati College of Medicine, Cincinnati, OH, USA
[9]Premium Research Institute for Human Metaverse Medicine (WPI-PRIMe), and Division of Stem Cell and Organoid Medicine, Osaka University, Suita, Osaka 565-0871, Japan
*Correspondence: takanori.takebe@cchmc.org
https://doi.org/10.1016/j.stemcr.2023.09.006

SUMMARY

UGT1A1 (UDP glucuronosyltransferase family 1 member A1) is the primary enzyme required for bilirubin conjugation, which is essential for preventing hyperbilirubinemia. Animal models lack key human organic anion transporting polypeptides with distinct epigenetic control over bilirubin metabolism, necessitating a human model to interrogate the regulatory mechanism behind UGT1A1 function. Here, we use induced pluripotent stem cells to develop human liver organoids that can emulate conjugation failure phenotype. Bilirubin conjugation assays, chromatin immunoprecipitation, and transcriptome analysis elucidated the role of glucocorticoid antagonism in UGT1A1 activation. This antagonism prevents the binding of transcriptional repressor MECP2 at the expense of NRF2 with associated off-target effects. Therefore, we introduced functional GULO (L-gulonolactone oxidase) in human organoids to augment intracellular ascorbate for NRF2 reactivation. This engineered organoid conjugated more bilirubin and protected against hyperbilirubinemia when transplanted in immunosuppressed Crigler-Najjar syndrome rat model. Collectively, we demonstrate that our organoid system serves as a manipulatable model for interrogating hyperbilirubinemia and potential therapeutic development.

INTRODUCTION

Neonatal hyperbilirubinemia is the yellowish discoloration of the skin and sclera due to high serum bilirubin levels, and it accounts for 114,000 annual deaths worldwide, particularly due to progression into severe cases with kernicterus (Olusanya et al., 2018). Nearly 50% of term and 80% of pre-term babies are afflicted with jaundice due to limited UGT1A1 activity around birth (Kumar, 1999; Watson, 2009). With proper treatment and care most of these cases are resolved. However, in some cases high levels of bilirubin cross the blood-brain barrier to cause kernicterus, which can result in permanent neurological damage and even death (Le Pichon et al., 2017).

Crigler-Najjar syndrome (CNS) is a rare form of hyperbilirubinemia caused by a loss-of-function mutation in the *UGT1A1* (UDP glucuronosyltransferase family 1 member A1) gene. The disease has an incidence of 1 in 1 million and is an inherited autosomal recessive disorder (Collaud et al., 2019). Treatment of hyperbilirubinemia involves multimodal therapy, which is centered around chronic daily phototherapy and augmented with close medical management (Gottimukkala et al., 2023). Although phototherapy can be effective with minimal risks, it poses a significant treatment burden for patients and families. In addition, acute exacerbations require hospitalization for hydration, intensive phototherapy, correction of electrolyte imbalances, and possible plasmapheresis or exchange transfusion (Bassari and Koea, 2015). Exchange transfusion in particular is associated with infection, metabolic and electrolyte abnormalities, and adverse transfusion reactions. Therefore, the only treatment for a complete cure is a liver transplant (Collaud et al., 2019).

Most severe cases of hyperbilirubinemia are caused by a lack of expression of UGT1A1 due to improper regulation of the gene. Glucocorticoid signaling has been widely linked to the regulation of UGT1A1, but there is conflicting evidence as to whether glucocorticoids are a positive regulator. Studies have indicated that glucocorticoids can activate PXR and hence UGT1A1, while others have suggested that higher hydrocortisone and hypercortisolism, i.e., excessive glucocorticoid, result in elevated bilirubin levels (Sugatani et al., 2005; Theiler-Schwetz et al., 2021; Werumeus Buning et al., 2016). Thus, the glucocorticoid-mediated regulatory mechanism behind UGT1A1 expression still eludes us.

Several advances have been made to generate model organisms for the study of UGT1A1 regulatory features

(Bortolussi and Muro, 2020). However, the epigenetic regulation of UGT1A1 in model organisms is different from that in humans in addition to the lack of vital transporter proteins for bilirubin uptake found in humans (van de Steeg et al., 2013). From a human perspective, primary human hepatocytes (PHHs), HepG2 and HepaRG cells have been used to model hyperbilirubinemia; however, reduced expression of UGT1A1 and relevant transporter proteins have made the process challenging (Hoekstra et al., 2013; Kammerer and Küpper, 2018). To solve this issue, induced pluripotent stem cell (iPSC)-derived hepatocyte-like cells have been used to mimic human bilirubin metabolism with varying success (Chen et al., 2015; Gao et al., 2017). Here, we use iPSC-derived human liver organoids (HLOs) as a personalized model system to study the disease and the mechanisms underpinning its regulation as it relates to the effect of glucocorticoid signaling and its subsequent epigenetic modulation of UGT1A1 (Kimura et al., 2022).

RESULTS

HLOs conjugate bilirubin using UGT1A1

We used the healthy iPSC lines to generate HLOs by differentiating them into definitive endoderm, directing them toward the posterior foregut, and eventually toward hepatic progenitors and HLOs (Figure S1A) (Ouchi et al., 2019; Shinozawa et al., 2021). These HLOs were used to model hyperbilirubinemia by treating the HLOs with varying concentrations of bilirubin (Figure 1A). The undifferentiated iPSCs expressed pluripotency markers such as SOX2 and OCT4, while the HLOs expressed differentiated liver markers such as HNF4A, AFP, ECAD, and SLCO1B1 after priming with 1 mg/L bilirubin (Figures S1B and 1B). The HLOs also expressed GCR and NCOR, which are nuclear receptor-related proteins thought to be important for the regulation of bilirubin metabolism (Figure 1B). These healthy HLOs have relatively lower expression of fetal liver markers such as *AFP*, *SOX9*, and *CDX2* while expressing relatively mature liver markers such as *ALB*, *MRP2*, *SLC4A2*, *HO-1*, *CYP3A4*, *G6PC*, *F7*, and *PXR* (Figures S1C–S1E). UGT1A1 is the rate-limiting enzyme for bilirubin conjugation in the liver. Upon treatment with bilirubin the healthy donor-derived HLOs had marked increase in expression of *UGT1A1* (up to >20-fold) with increasing concentration of bilirubin treatment (Figure 1C). UGT1A1 was specific to the PROX1+ hepatocytes in the HLOs, which also expressed ALB (Figure S1F). These HLOs exhibited lower expression of CDX2 with bilirubin treatment relative to human intestinal organoids (Figures S1G–S1I). The organoids started accumulating bilirubin in their lumens, which grew darker over time when compared with control HLOs upon bilirubin treatment (Figure 1D).

Loss and restoration of bilirubin conjugation ability in CNS iPSC-derived HLOs

We next sought to test if HLOs can emulate patients' conditions that have a genetic bilirubin conjugation defect such as CNS type 1. We identified a 24-year-old Japanese male patient who had exhibited severe jaundice, unconjugated hyperbilirubinemia, and growth retardation since immediately after birth (Aono et al., 1994). The patient was unresponsive to phototherapy and phenobarbital, and underwent auxiliary partial orthotopic living donor liver transplantation with a graft from his mother when he was 5 years old (Figure S2A). A genetic analysis of peripheral blood mononuclear cells (PBMCs) from the patient revealed a point mutation in exon 1 of the *UGT1A1* gene. We sequenced the *UGT1A1* gene of this patient and found a nonsense mutation, c.858C>A (p.Cys280X), compared with healthy iPSCs and PHHs (Figure S2B). We proceeded to generate a stable iPSC line from PBMCs of this patient using episomal plasmids and generated HLOs by differentiating them into definitive endoderm (Figures S2C and S2D). The CNS iPSCs exhibited regular pluripotency markers such as SOX2 and OCT4, which were identical to healthy iPSCs. The CNS HLOs were again virtually identical to healthy HLOs, expressing HNF4A, AFP, ALB, PROX1, and ECAD with consistent cellular diversity as seen with flow cytometry when compared with controls (Figures S2E–S2I). The HLOs, however, lacked UGT1A1 expression as expected. On treatment with bilirubin the CNS HLOs failed to accumulate bilirubin in their lumens efficiently and filled with debris over time (Figure 1E). We further performed a UGT activity assay and found that healthy HLOs had 4.75 mU/mg activity compared with 7 mU/mg in PHHs, while CNS HLOs did not exhibit any detectable activity (Figure 1F). In addition, a bilirubin assay revealed that CNS HLOs failed to conjugate bilirubin, while the healthy HLOs exhibited about 2.45 ± 0.1 mg/L conjugated bilirubin (Figure 1G). To test if this phenotype is induced by defective UGT1A1, we transfected human *UGT1A1* mRNA into the CNS HLOs. The transfected HLOs were able to accumulate bilirubin within their lumens and conjugated bilirubin (3.75 ± 0.2 mg/L) more efficiently than non-transfected CNS HLOs (Figures S2J and S2K). Together, the organoid demonstrates UGT1A1 activity and subsequent conjugation capacity, which are sufficient to distinguish CNS pathology, rescued by *UGT1A1* mRNA restoration.

UGT1A1 is negatively regulated by MECP2-mediated glucocorticoid signaling

Since glucocorticoids have been implicated to regulate UGT1A1, we decided to treat the bilirubin-exposed HLOs with glucocorticoid agonists (hydrocortisone and dexamethasone) and antagonists (ketoconazole and mifepristone) to further elucidate the regulation of UGT1A1. We

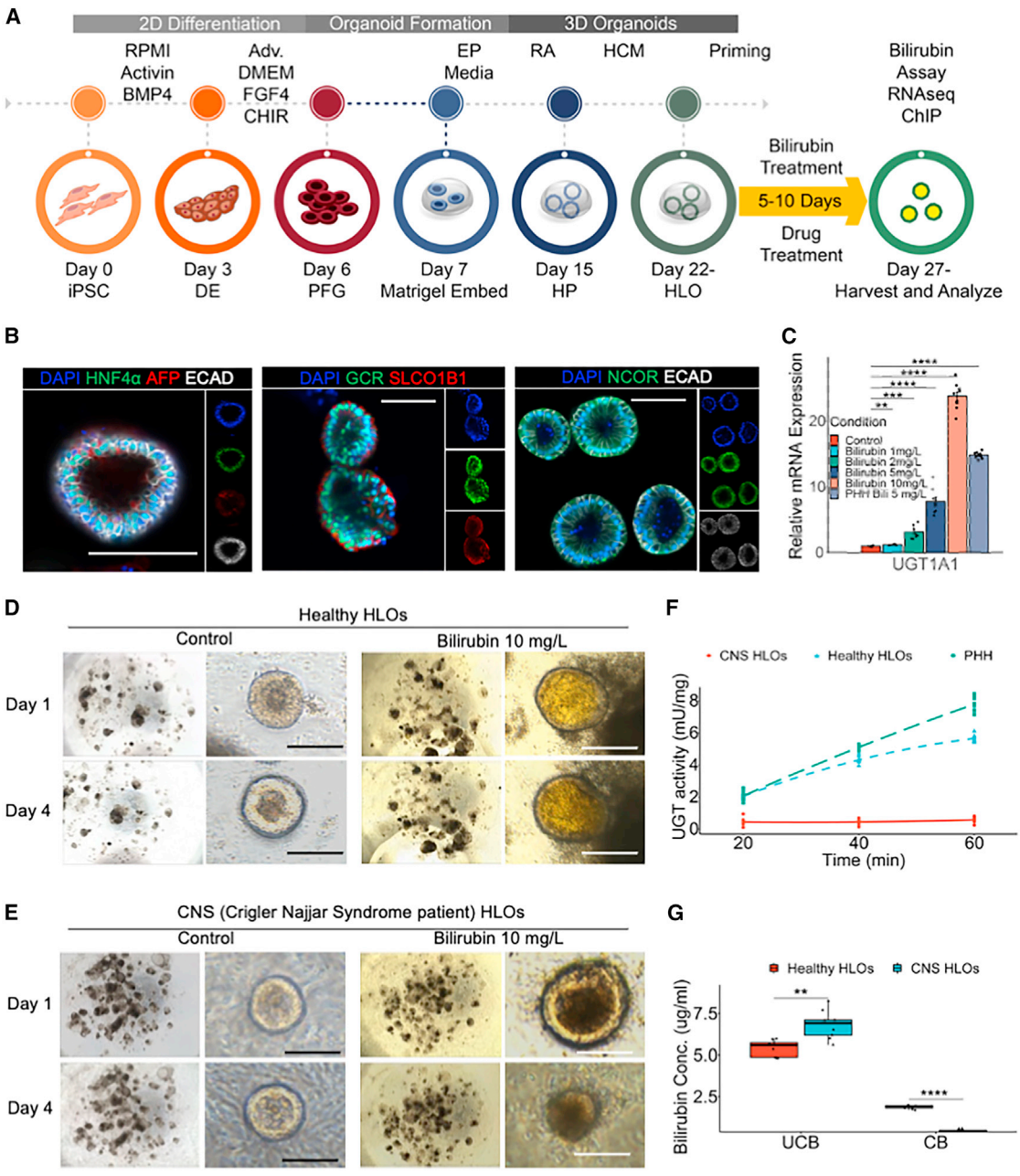

Figure 1. Human liver organoid (HLO) from iPSC carrying functional UGT1A1 conjugate bilirubin

(A) Schematic for generation of HLOs and bilirubin treatment.

(B) Immunofluorescence images of healthy HLOs for HNF4α, AFP, GCR, SLCO1B1, NCOR, and ECAD. Scale bars, 200 μm.

(C) qRT-PCR of *UGT1A1* gene for organoids treated with varying concentrations of bilirubin compared with untreated organoids and PHH. Data are mean $\pm$ SD, n = 9 independent experiments.

(D) Bright-field image of healthy HLOs treated with bilirubin (10 mg/L) compared with control after 1 and 4 days. Scale bars, 200 μm.

(E) Bright-field image of CNS HLOs treated with bilirubin (10 mg/L) compared with control after 1 and 4 days. Scale bars, 200 μm.

(F) UGT activity assay comparing healthy and CNS HLOs to PHH. n = 9 independent experiments.

(G) Bilirubin assay measuring unconjugated and conjugated bilirubin in healthy and CNS HLOs. n = 9 independent experiments.

ns, $p > 0.05$, *$p \leq 0.05$, ** $p \leq 0.01$, ***$p \leq 0.001$, and ****$p \leq 0.0001$.

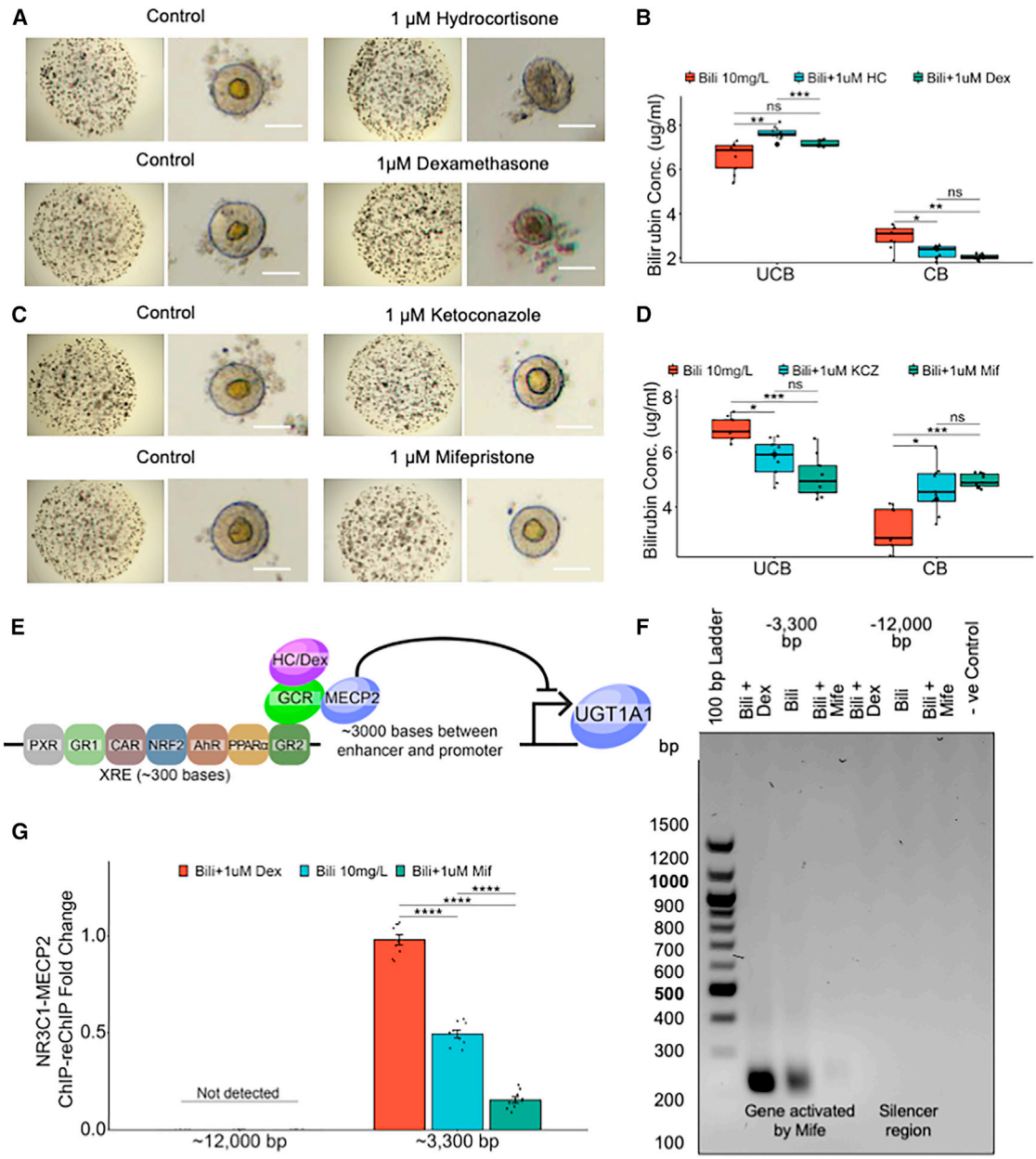

Figure 2. UGT1A1 is negatively regulated by glucocorticoid signaling

(A) Bright-field images of organoids treated with 10 mg/L bilirubin and agonists: hydrocortisone (1 μM) and dexamethasone (1 μM). Scale bars, 200 μm.

(B) Bilirubin assay measuring unconjugated and conjugated bilirubin in the samples in (A). n = 9 independent experiments.

(C) Bright-field images of organoids treated with 10 mg/L bilirubin and antagonists: ketoconazole (1 μM) and mifepristone (1 μM). Scale bars, 200 μm.

(D) Bilirubin assay measuring unconjugated and conjugated bilirubin in the samples in (C). n = 9 independent experiments.

(E) Schematic for XRE element upstream of *UGT1A1* gene depicting how GCR and MECP2 affect expression of UGT1A1.

(F) NR3C1-MECP2 ChIP-reChIP-PCR for organoids treated with 10 mg/L bilirubin and mifepristone (1 μM) or dexamethasone (1 μM).

(G) NR3C1-MECP2 ChIP-reChIP-qPCR for samples in (F). Data are mean ± SD, n = 9 independent experiments.

ns, $p > 0.05$, *$p \leq 0.05$, **$p \leq 0.01$, ***$p \leq 0.001$, and ****$p \leq 0.0001$.

first treated the HLOs with varying concentrations of the agonists and antagonists and found the most effective non-toxic dose to be 1 μM (Figures S3A and S3B). With dexamethasone treatment, the glucocorticoid receptor (NR3C1) was re-localized from the cytoplasm to the nucleus suggesting an active pathway (Figure S3C). Additionally, the *NR3C1* gene expression level was comparable with PHHs (Figure S3D). We found that HLOs treated with the agonists failed to conjugate bilirubin (control = 2.92 vs. hydrocortisone = 2.03 and dexamethasone = 2.28 mg/L) (Figures 2A and 2B). On the other hand, HLOs treated with the antagonists remained healthy and conjugated bilirubin efficiently (control = 3.19 vs. ketoconazole = 4.66 and mifepristone = 4.95 mg/L) (Figures 2C and 2D). The UGT1A1 gene has a xenobiotic response element (XRE) 3,000 bp upstream of its promoter region where several nuclear receptors bind to regulate the expression. The XRE houses glucocorticoid receptor binding sites in close proximity to MECP2 binding sites, which can potentially repress the expression of UGT1A1 (Figure 2E). Therefore, to test our hypothesis, we performed a ChIP-PCR and ChIP-qPCR for MECP2, a potent transcriptional inhibitor, and found a significant drop in repression with mifepristone treatment when compared with dexamethasone treatment (0.5- vs. 2-fold difference) (Figures S3E and S3F). Furthermore, to test the binding of NR3C1 to these MECP2 bound sites, we performed a ChIP-reChIP-PCR and ChIP-reChIP-qPCR for NR3C1 and MECP2 (Figures 2F and 2G). These data suggest that glucocorticoid receptors can recruit MECP2 for inhibition of UGT1A1 expression, while its antagonists can be used to inhibit recruitment of MECP2 and rally UGT1A1 expression.

RNA sequencing reveals importance of ROS and xenobiotic metabolism in bilirubin uptake and conjugation

We opted to further elucidate the regulation of bilirubin metabolism with an RNA sequencing (RNA-seq) experiment comparing the mifepristone-treated samples with the control and found that, while xenobiotic metabolism genes such as *UGT1A1*, *BLVRA*, and *SOD1* were upregulated, transporter proteins such as *OATP2*, *ABCC2*, and *ABCC3* were downregulated. In addition, inflammatory and fibrotic genes such as *IL-6*, *IL-8*, *IL-1β,* and *VIM* (Figures 3A and 3B). A GSEA (Gene Set Enrichment Analysis)showed that several important pathways including pigment metabolism were significantly overexpressed (Figure 3C). However, in addition to metabolism of xenobiotics and bile secretion, several other pathways such as fat digestion and metabolism and steroid biosynthesis were upregulated (Figure 3D). While glucocorticoid antagonists enhance bilirubin conjugation, this is at the expense of bilirubin uptake through transporter proteins and induction of inflammatory responses. Therefore, to identify target genes that can prevent such off-target responses, we performed a cross-comparison of xenobiotic and ROS (Reactive Oxygen Species) metabolism in a GSEA (Figure 3E). The GSEA showed that several important genes were upregulated while some significant genes were downregulated or not active; however, we identified *NRF2* as the key gene that was involved in both processes to be not upregulated (Figure 3F). Most of the other genes found such as *AKR1C3*, *AOC1*, *CES2*, and *CYP46A1* were downstream of *NRF2*, while most pan-hepatic genes such as *AFP*, *PROX1*, and *ALB* remain unchanged (Figures S3G and S3H). Since *NRF2* is a known master regulator of detoxification and antioxidant activity in the liver, there might be a possibility to protect from oxidative stress in the HLOs while maintaining bilirubin metabolism.

mGULO HLOs conjugate bilirubin using UGT1A1

Vitamin C or ascorbate is a well-known activator of NRF2 signaling, which in turn induces detoxification and antioxidant activity that is very important in debilitating diseases such as hyperbilirubinemia (Kim et al., 2015; Mostafavi-Pour et al., 2017). Vitamin C has been used as a supplement to treat hyperbilirubinemia with modest benefits (Khadem al-hosseini et al., 2020). However, due to lack of a functional GULO (*L-gulonolactone oxidase*) gene in humans (Cui et al., 2011), ascorbate needs to be taken as a dietary supplement to reap its benefits. Intracellular absorption by mammalian cells relies on SVCT and GLUT transporter proteins, thereby limiting the uptake due to saturation of the transporter proteins (Savini et al., 2008). Therefore, we used a synthetic biology approach to knock in the murine form of active *GULO* (*mGULO*) gene with a P2A mCherry under a Tet ON system into healthy iPSCs to augment intracellular ascorbate availability. The engineered HLOs (eHLOs) expressed the mGULO gene along with mCherry and synthesized intracellular vitamin C upon treatment with doxycycline (Dox) (Figure 4A). Dox-induced mCherry expression at the HLO stage was about 94% (Figure S2F). Flow cytometric profiling showed 70% of cells in eHLOs are ALB+ hepatocyte-like cells as was seen in conventional HLOs from other cell lines (Figures S2G and S2H). The eHLO cells were stable and expressed similar levels of *AFP* to control HLOs while expressing high levels of *mGULO* (Figures S4A and S4B). With varying Dox concentrations, we observed marked increase of bilirubin accumulation in the lumen of the eHLOs (Figure 4B, top).

Next, we wanted to verify the bilirubin accumulation using the green fluorescent UnaG probe (Kumagai et al., 2013), which specifically binds to unconjugated bilirubin, and observed significant increase in fluorescence inside the lumen when eHLOs were treated with the bilirubin (Figure 4B, bottom). This observation was

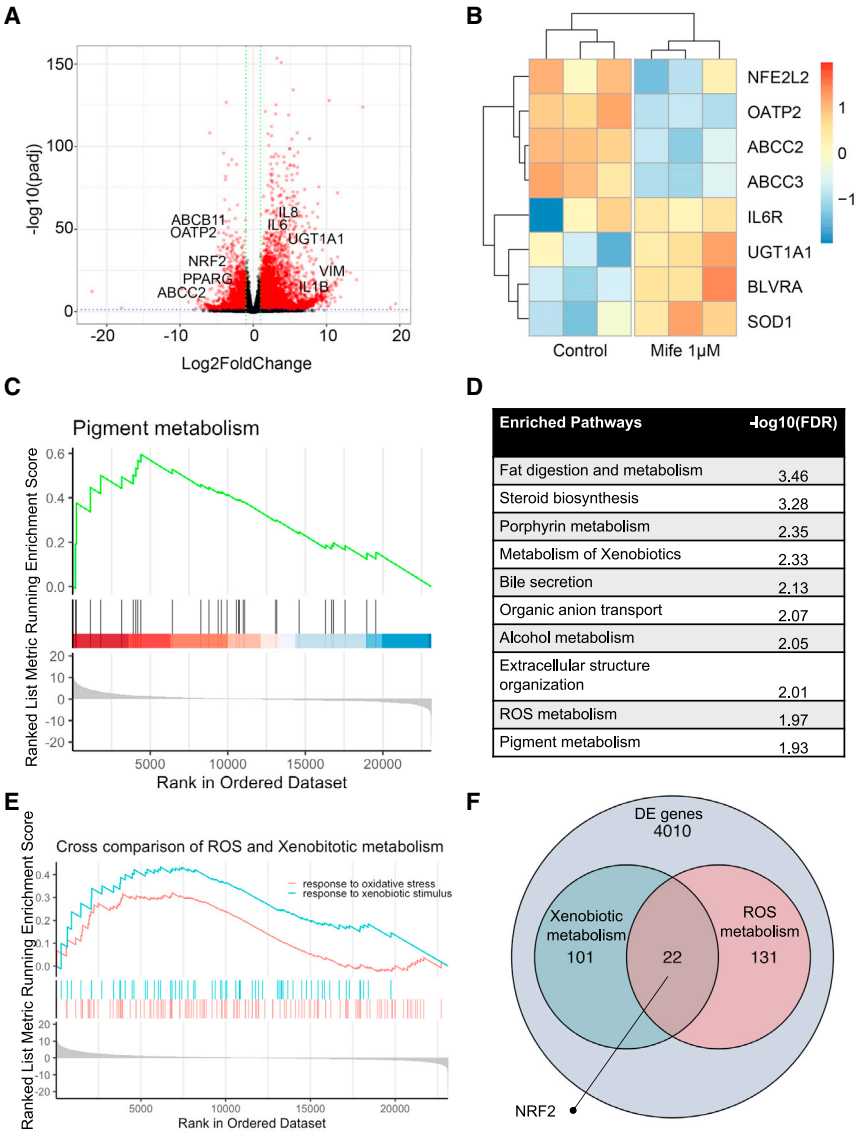

Enriched Pathways	-log10(FDR)
Fat digestion and metabolism	3.46
Steroid biosynthesis	3.28
Porphyrin metabolism	2.35
Metabolism of Xenobiotics	2.33
Bile secretion	2.13
Organic anion transport	2.07
Alcohol metabolism	2.05
Extracellular structure organization	2.01
ROS metabolism	1.97
Pigment metabolism	1.93

Figure 3. RNA-seq reveals importance of ROS and xenobiotic metabolism in bilirubin uptake and conjugation

(A) Volcano plot for differentially expressed genes in mifepristone-treated organoids compared with control after treatment with bilirubin. Key genes are highlighted.

(B) Heatmap for mifepristone-treated organoids compared with control after treatment with bilirubin.

(C) GSEA plot depicting enhanced pigment metabolism in mifepristone-treated organoids.

(D) Enriched pathways in mifepristone-treated organoids.

(E) Cross comparison of ROS and xenobiotic metabolism pathway in a GSEA.

(F) Venn diagram depicting NRF2 as a key gene important for both xenobiotic and ROS metabolism.

corroborated by the bilirubin assay, which indicated significant increase in conversion of unconjugated to conjugated bilirubin when treated with increasing concentration (10–1,000 ng/mL) of Dox, with 100 ng/mL being the ideal concentration (conjugated bilirubin = 6.02 ± 0.05 mg/L) (Figure 4C). Comparatively, no obvious improvement was observed with 100 ng/mL Dox treatment in wild-type HLOs (Figure S4C). However, the mCherry+ eHLOs exhibited expression of NRF2, MRP2, MDR1, ALB, ASGR1, ECAD, and UGT1A1 in the PROX1+ hepatocytes (Figures S4D and S4E). In addition, we observed that the lumen of some eHLOs was not fluorescent even though they had accumulated significant amounts of bilirubin indicated by the dark brown coloration. Since UnaG does not bind conjugated bilirubin, this indicates that the loss of fluorescence was due to the accumulation of conjugated bilirubin (Figure 4D). The HLOs were also able to uptake fluorescent bile acid readily into their lumen validating the UnaG results since bile acids are transported in a similar directionality to bilirubin (Figure S4F). The eHLOs treated with Dox 100 ng/mL exhibited higher expression of NRF2 (4.7-fold) and lower expression of IL-6 (0.5-fold), indicating a more robust xenobiotic response while maintaining low inflammation (Figure 4E). Finally, we measured the organoid viability and the eHLOs that contained conjugated bilirubin and found that Dox treatment significantly enhanced both viability and conjugation (>75% and >50%, respectively) (Figure 4F). Therefore, genetic *GULO* activation in organoids enhanced bilirubin conjugation compared with glucocorticoid perturbation.

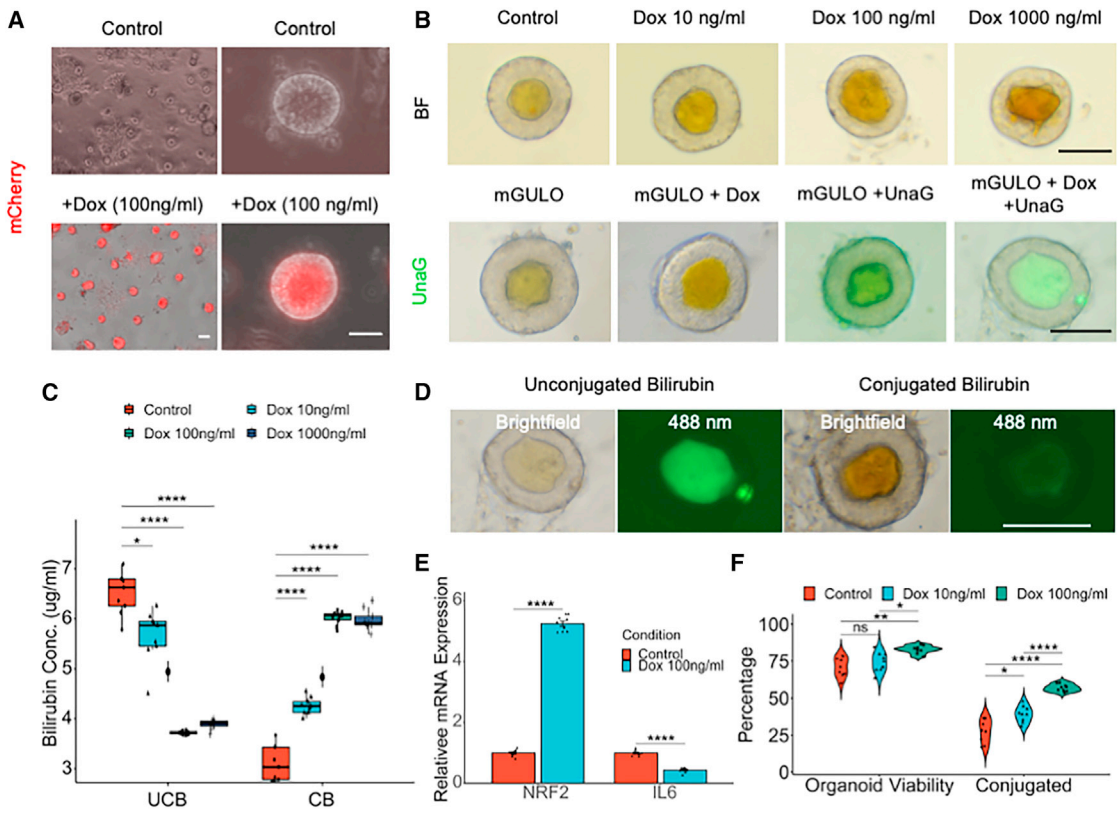

Figure 4. Active GULO carrying eHLOs conjugate bilirubin more efficiently

(A) Bright-field and fluorescence images of mCherry expression in Dox-treated mGULO HLOs compared with control HLOs. Scale bar, 200 μm.

(B) Bright-field image of mGULO HLOs treated with bilirubin (10 mg/L) and Dox (0–1,000 ng/mL) (top). UnaG assay for mGULO organoids treated with Dox compared with control (bottom). Scale bars, 200 μm.

(C) Bilirubin assay measuring unconjugated and conjugated bilirubin in mGULO HLOs treated with bilirubin (10 mg/L) and Dox (0–1,000 ng/mL). n = 9 independent experiments.

(D) UnaG assay shows conjugation of bilirubin indicated by loss of fluorescence even in the presence of dark yellow bilirubin. Scale bar, 200 μm.

(E) qRT-PCR of *NRF2* and *IL6* gene for mGULO organoids treated with Dox (100 ng/mL) compared with control after treatment with bilirubin. Data are mean ± SD, n = 9 independent experiments.

(F) Total percentage of viable organoids and organoids carrying conjugated bilirubin in Dox-treated organoids compared with control. n = 9 independent experiments.

ns, $p > 0.05$, *$p \leq 0.05$, **$p \leq 0.01$, ***$p \leq 0.001$, and ****$p \leq 0.0001$.

Orthotopic transplantation of eHLOs alleviates hyperbilirubinemia in rodents

Finally, we wanted to test whether the eHLOs were functional in an *in vivo* setting and transplanted them into the portal vein of Gunn rats to treat them (Figure 5A). In a time course experiment, we found that the human albumin in the Gunn rat serum peaked rapidly (527 ± 32 ng/mL) at around 30 days after transplantation and persisted until at least 60 days (Figure 4B). Reduction of modestly elevated AST and ALT has been observed by serum biochemistry assays (approximately 8% and 6% drop) (Figures S5A and S5B). Longitudinal bilirubin measurements showed that there was an almost 30% peak drop in bilirubin level in Gunn rats transplanted with eHLOs at about day 40 and this improvement persisted longer relative to normal HLOs (Figure 5C). Taken together, orthotopic transplantation of eHLOs reduced bilirubin levels in animals suffering from hyperbilirubinemia.

DISCUSSION

Here, we have developed a new organoid-based platform for studying the development and disease mechanism for

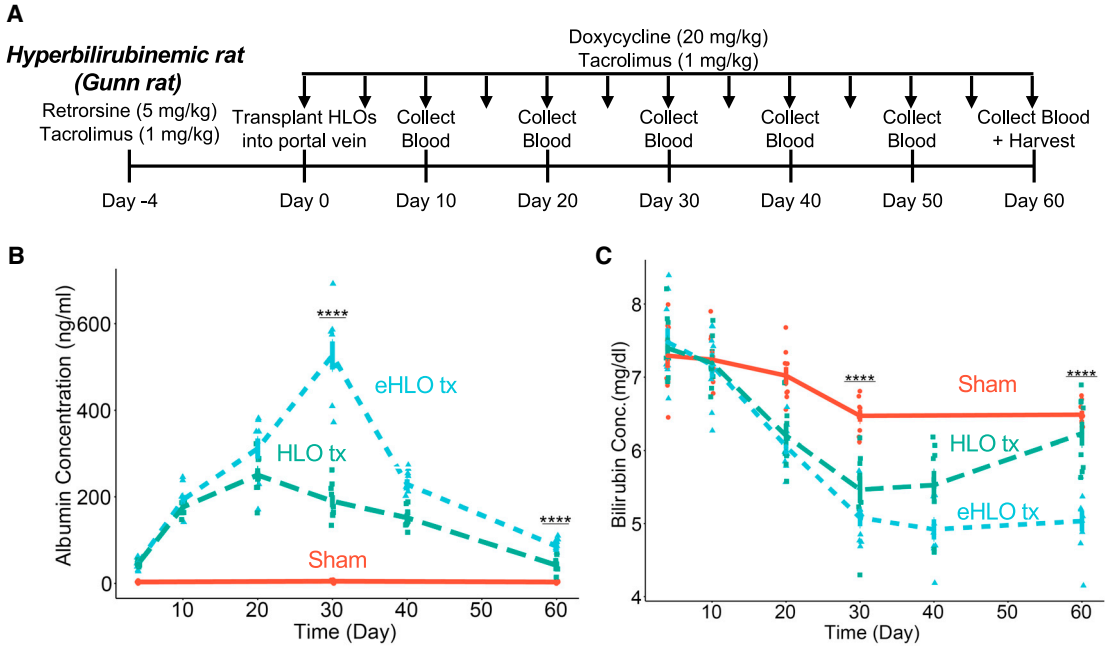

Figure 5. Orthotopic eHLO transplantation alleviates hyperbilirubinemia in rats

(A) Experimental timeline for orthotopic transplantation of HLOs in rats.

(B) Human albumin ELISA on blood serum collected from rats at different time points after transplantation. n = 9 independent experiments.

(C) Bilirubin assay on blood serum collected from rats at different time points after transplantation. n = 9 independent experiments.

ns, $p > 0.05$, *$p \leq 0.05$, **$p \leq 0.01$, ***$p \leq 0.001$, and ****$p \leq 0.0001$.

human bilirubin metabolism. The HLOs express arrays of proteins such as GCR, SLCO1B1, NCOR, and MRP2, which are inherent to bilirubin metabolism in the human liver and some of which are not found in rodents (Zhang et al., 2007). The HLOs treated with modest bilirubin dosage exhibit lower AFP expression compared with conventional HLOs while maintaining UGT1A1 activity at a level of PHH. In support, this UGT1A1 activity is lacking in the CNS samples using patient-derived cell lines. The bilirubin-primed HLOs had reduced CDX2 expression, suggesting a shift toward a more hepatic rather than intestinal character. Our data suggest that the organoids take up bilirubin in the hepatocytes using the SLCO1B1 transporter protein (localized to the basolateral outer side of the HLO), which is known to take up unconjugated bilirubin in the native liver and mutations in the gene results in Rotor syndrome. The bilirubin is conjugated by UGT1A1 and transported to the lumen by MRP2 (conjugated bilirubin transporter), while excess unconjugated bilirubin is sequestered in the lumen of the organoids via MDR1 (an unconjugated bilirubin transporter, located on the apical luminal side of HLOs) (Shinozawa et al., 2021). We have shown that these liver organoids can be used to model and correct the CNS phenotype, indicating the functional conjugation capability. We also showed the feasibility of mRNA (UGT1A1) or genetic manipulation (inducible mGULO) that can modify the bilirubin metabolism pathway in organoids without affecting the character or cellular diversity of the organoids. Therefore, as the system we have developed is highly manipulable and tractable, liver organoids will offer a foundation for investigating the impact of bilirubin on a diverse population of cells with synthetic gene modification.

Glucocorticoids have been linked to bilirubin metabolism and UGT1A1 expression for a long time, and Kobayashi et al. (2022) have shown that this effect depends on the concentration of the glucocorticoid agonists. The glucocorticoid receptor agonist dexamethasone has been shown to act as a competitive inhibitor of CYP3A4 in a dose-dependent manner (Relling et al., 1994). In addition, dexamethasone is involved in the formation of a repression complex consisting of glucocorticoid receptors, MECP2 and HDAC1 (Sharma et al., 2013). Further evidence indicates that inhibition of NRF2 mediated by an increase in HDAC activity and increased binding of transcriptional repressor MECP2 at CpG sites at the promoter region is what could lead to UGT1A1 repression (Khor et al., 2014). In our experimental system, since the standard organoid culture medium contains dexamethasone to induce growth and reduce

inflammation of HLOs; additional supplementation beyond the equilibrium results in reduced bilirubin conjugation. In fact, inhibition of glucocorticoid signaling results in enhanced bilirubin conjugation. To interpret the underlying mechanism behind these observations, we found that excess glucocorticoid signaling results in recruitment of MECP2 near the XRE of the UGT1A1 glucocorticoid receptor binding site. This deployment results in transcriptional repression, but the repression can be overcome by supplementation with glucocorticoid inhibition, with compounds such as ketoconazole and mifepristone.

These glucocorticoid antagonists, however, are hepatotoxic in higher concentration, with a wide range of hormonal effects (Bhasin et al., 1986; Sai et al., 2019). Indeed, in the HLOs, the antagonists seem to induce UGT1A1 expression at the expense of bilirubin transporter proteins and inflammatory milieu while hepatocyte-specific genes remain unchanged. To overcome these issues, RNA-seq analysis of glucocorticoid-inhibited organoids identified NRF2 as a master regulator of detoxification and antioxidant activity in the liver (Pall and Levine, 2015), which can be directly activated by vitamin C (Xu et al., 2020), to enhance xenobiotic metabolism (Martin, 2010; Mitsuishi et al., 2012). In support, UGT1A1 is known to be regulated by the activity of NRF2 (Yueh and Tukey, 2007). Alam et al. (2017) have suggested that glucocorticoid signaling represses the transcriptional transactivation mediated by NRF2 by inhibit histone acetylation. Since NRF2 transactivation is inhibited following high glucocorticoid levels, NRF2 activators such as ascorbate can be used to lift this suppression of UGT1A1. However, as human cells do not produce vitamin C, we decided to generate mGULO-carrying iPSC-derived HLOs to overcome off-target issues associated with glucocorticoids. GULO genetic activation increased expression of NRF2 in these engineered HLOs or eHLOs without inflammatory responses. The mCherry+ eHLOs were more efficient at conjugating bilirubin, while maintaining high viability, presumably due to the expression of UGT1A1 and the transporter proteins MDR1 and MRP2. Milder forms of hyperbilirubinemia such as breast milk jaundice and fasting are known to result in increased systemic glucocorticoid concentration. Our data support the hypothesis that hyperbilirubinemia is caused by this increase in glucocorticoids that mediates NRF2 downregulation. Given that breastmilk contains high levels of glucocorticoids and fasting induces increased glucocorticoids immediately after commencement, the excessive glucocorticoids might induce suppression of UGT1A1 and eventually neonatal hyperbilirubinemia (Kim et al., 2021; Pundir et al., 2020). As HLOs contain both parenchymal and non-parenchymal lineages (Ouchi et al., 2019; Shinozawa et al., 2021), cell types other than hepatocytes could potentially contribute to the glucocorticoid antagonist-mediated activation of pro-inflammatory and pro-fibrotic genes. Therefore, the potential role of non-cell-autonomous effects demands further investigation to elucidate the mechanism behind multicellular responses.

The only definitive cure for severe forms of hyperbilirubinemia such as CNS is liver transplantation (Tcaciuc et al., 2021). Several studies have reported the transplantation of hepatocyte-like cells and there is alleviation of disease symptoms after 4 weeks (Chen et al., 2015; Fourrier et al., 2020; Gao et al., 2017; Maerckx et al., 2014; Peterson et al., 2019). Our liver organoids are able to survive for several months while providing the functionality required for treatment of CNS, and the alleviation of the disease symptoms starts around 10 days post transplantation. The eHLOs produce human albumin up to 60 days after transplantation into an immunocompetent CNS rat model with a regimen of immunosuppressants. In addition, the organoids provide therapeutic benefits in removing excess bilirubin and improving liver functions initiated upon 10 days of transplantation. Comparatively, most studies showed a prolonged bilirubin removal up until 196 days; however, it should be noted that the reports injected 10^6 to 10^7 induced hepatocyte-like cells compared with our injection 5×10^5 HLO cells. Despite being modest dosing, our results show a similar response in bilirubin removal (~30% down to 5 mg/dL) until 30 days after transplantation. In terms of bilirubin removal, the eHLOs performed better when compared with regular HLOs due to their enhanced redox maintenance which increased survivability of organoids and enhanced bilirubin metabolism, which peaked at day 40 but was observable even at day 60. The efficacy duration is, however, weakened beyond day 60, likely aggravated by a combination of xenorejection and bile autotoxicity. Therefore, further investigations are required to delineate the exact mechanism for durable engraftment and to develop more robust cellular therapies that can evade xenorejection and bile autotoxicity. Nevertheless, our data argue that engineered organoid transplantation can be a potential bridging option to liver transplantation for severe hyperbilirubinemia diseases.

EXPERIMENTAL PROCEDURES

Resource availability

Corresponding author

Further information and requests for resources and reagents should be directed to and will be fulfilled by the corresponding author, Takanori Takebe (takanori.takebe@cchmc.org).

Materials availability

Materials, cell lines, and additional details can be made available by the corresponding author upon reasonable request.

Data and code availability

The RNA-seq data reported in this paper have been deposited to the NCBI Gene Expression Omnibus (GEO) with the following accession no. GSE222362. Reference codes for bioinformatics analyses can be found at the following link: https://github.com/hasanwraeth/RNAseq. All other data supporting the findings of this study are available from the corresponding author on reasonable request.

Animals

All animal experiments were conducted with the approval of the Institutional Review Board (IRB) and Institutional Animal Care and Use Committee of the Cincinnati Children's Hospital Medical Center. Adult Gunn (Gunn-Ugt1a1j/BluHsdRrrc) rats (breeding pairs, 9–12 weeks old) were obtained from the Rat Resource & Research Center (RRRC, Columbia, MO). Rats were housed in standard rat cages with woodchip bedding, maintained at a temperature of 20°C–24°C and relative humidity of 45%–55%, under a 12 h light/12 h dark cycle. All animals had *ad libitum* access to standard chow (Cincinnati Lab Supply, Cincinnati, OH) before study. All animals were treated in accordance with the guidelines and regulations of the institution.

mGULO editing

All experiments concerning human agents and subjects were conducted with the approval of Institutional Biosafety Committee (IBC) and Institutional Review Board (IRB) at CCHMC. The murine GULO (L-gulonolactone oxidase) cDNA sequence was retrieved from NCBI. The 5′ linker and Kozak sequence were added to the start of the sequence, with HA tags to the end of the sequence. In addition, a P2A-mCherry was added after the HA tag and a 3′ linker to the very end. The custom gene was then synthesized and cloned into the pAAVS1-NDi-CRISPRi (Gen1) PCSF no. 117 vector using the restriction sites AflII and AgeI. The vector has a TetON system and a Neo^r selectable marker was then inserted using Gateway technology.

CNS and mGULO iPSC generation and general iPSC maintenance

The CNS iPSC line was derived from a patient with CNS under IRB approved by Kyoto University, while the mGULO iPSC line was generated by inserting the modified GULO sequence into the AAVS1 site of CuSTOM1 iPSC line. The generation and maintenance of the iPSC lines are described in more detail in supplemental information.

Organoid generation

The generation of organoids is described in supplemental information.

HLO treatment with bilirubin and drugs

The HLOs were primed with 1 mg/L bilirubin on day 22 prior to further bilirubin treatment for acclimatization. On day 27, the mature organoids were treated with bilirubin (1–10 mg/L), Dox (100 ng/mL) (added 3 days prior as well to activate gene expression), and drugs such as hydrocortisone, dexamethasone, ketoconazole, and mifepristone (1–2 μM for each) for 5 days after deprivation of dexamethasone for 2 days before treatment and then harvested for downstream assays.

Transfection of mRNA into HLOs

For transfection, the CNS HLOs were isolated by breaking up the Matrigel droplets with a pipette and washed with PBS three times. The HLOs were resuspended with Lipofectamine 3000 (Invitrogen) and Opti-MEM I (Gibco) containing 10 μg UGT1A1 and mCherry mRNA constructs and incubated at 37°C for 2 h. After 2 h, the organoids were re-embedded in Matrigel and fed with fresh HCM.

Organoid transplantation into the portal vein

The eHLOs and regular HLOs were harvested on day 27 and dissociated into chunks by repeated pipetting, washed with PBS, and resuspended with HCM containing 2% FBS and CEPT (Chroman 1, Emricasan, Polyamines, and Trans-ISRIB, Bio-Techne) cocktail to increase viability. The recipient rats were treated with a single intraperitoneal dose of retrorsine (5 mg/kg) and tacrolimus (0.8 mg/kg) 4 days before the transplantation. On the day of surgery, an exploratory laparotomy was performed via midline incision followed by bowel evisceration to expose the portal triad, including the portal vein. With the portal vein exposed, a 32G 1 inch needle was used to inject 3×10^3 organoids (roughly 5×10^5 cells) in a 200-μL infusion into the portal vein. Bleeding was controlled by application of a bulldog clamp distal to the site of injection. This also assisted with preferential flow into the liver. Excessive blood loss was controlled by application of a SURGICEL SNoW Absorbable Hemostat (Ethicon). The incision was then closed in two layers with 5-0 vicryl-coated surgical sutures (Ethicon) and GLUture (Zoetis) and buprenorphine (0.1 mg/kg) was administered as an analgesic. The animal was then maintained on Dox (20 mg/kg) and tacrolimus injections every 3–4 days until the day of harvest. Blood was collected regularly by the retro-orbital method as needed.

Quantification and statistical analysis

Statistical analyses were mainly performed using R software v.4.2.0 with unpaired two-tailed Student's t test, one-way Anova and post hoc Tukey's test, or Welch's t test. Statistical analyses for non-normally distributed measurements were performed using non-parametric Kruskal-Wallis and post hoc Dunn-Holland-Wolfe tests. For comparisons between unpaired groups, when groups were independent and the variances were unequal, a non-parametric Brunner-Munzel test was performed, unless noted otherwise. p values <0.05 were considered statistically significant. n values refer to biologically independent replicates. The image analyses were non-blinded. Statistical parameters are in the figures and figure legends, where: ns, $p > 0.05$, *$p \leq 0.05$, **$p \leq 0.01$, ***$p \leq 0.001$, and ****$p \leq 0.0001$. Using G*Power software, for each experiment, we determined the minimum sample size to collect the data for using the preliminary effect sizes, $\alpha = 0.05$ and power = 0.8. For all experimental data, we also conducted a post hoc power analysis to determine whether our design had enough power. We had enough power (power >0.8) for all our experiments.

SUPPLEMENTAL INFORMATION

Supplemental information can be found online at https://doi.org/10.1016/j.stemcr.2023.09.006.

ACKNOWLEDGMENTS

We would like to thank Atsushi Miyawaki, Laboratory for Cell Function and Dynamics, Brain Science Institute, RIKEN, for providing us with the UnaG protein for analysis of bilirubin. We also thank all other Takebe lab members for their support. This work was supported by Cincinnati Children's Research Foundation grant, the Falk Transformational Awards Program, NIH Director's New Innovator Award (DP2 DK128799-01) and CREST (20gm1210012h0001) grant from Japan Agency for Medical Research and Development (AMED) to T.T. This work was also supported by an NIH grant UG3/UH3 DK119982, Cincinnati Center for Autoimmune Liver Disease Fellowship Award, PHS Grant P30 DK078392 (Integrative Morphology Core and Pluripotent Stem Cell and Organoid Core) of the Digestive Disease Research Core Center in Cincinnati, Takeda Science Foundation Award, Mitsubishi Foundation Award, and AMED grants JP23bm1223006, JP23bm1123009, JP23gm1210012, JP23fk0210106, JP23fk0210091, JP18fk0210037, JP18bm0704025, JP21bm0404045, and JP21fk0210060, JST Moonshot JPMJMS2022-10 and JPMJMS2033-12, and JSPS KAKENHI Grant JP21H04822, JP18H02800, 19K22416. T.T. is a New York Stem Cell Foundation – Robertson Investigator. We would also like to acknowledge the CCHMC Confocal Imaging Core (RRID: SCR_022628), Pathology Research Core (RRID:SCR_022637), Pluripotent Stem Cell Facility (RRID:SCR_022634), Transgenic Animal and Genome Editing Core (RRID:SCR_022642), Veterinary Services Facility, and Research Flow Cytometry Core (RRID: SCR_022635). Finally, we would also like to acknowledge the thesis committee for HAR for their continued support and constructive criticism.

AUTHOR CONTRIBUTIONS

H.A.R. designed and performed the research, analyzed data, performed the bioinformatics analyses, and wrote the paper. Z.F., A.A.R., and C.C. conducted the research and revised the paper. K.I. designed the research and revised the paper. Y.O., K. Okita, and K. Osafune conducted the research. T.T. designed the research and wrote the paper.

DECLARATION OF INTERESTS

The authors declare no competing interests.

Received: January 24, 2023
Revised: September 13, 2023
Accepted: September 14, 2023
Published: October 12, 2023

REFERENCES

Alam, M.M., Okazaki, K., Nguyen, L.T.T., Ota, N., Kitamura, H., Murakami, S., Shima, H., Igarashi, K., Sekine, H., and Motohashi, H. (2017). Glucocorticoid receptor signaling represses the antioxidant response by inhibiting histone acetylation mediated by the transcriptional activator NRF2. J. Biol. Chem. *292*, 7519–7530. https://doi.org/10.1074/jbc.M116.773960.

Aono, S., Yamada, Y., Keino, H., Sasaoka, Y., Nakagawa, T., Onishi, S., Mimura, S., Koiwai, O., and Sato, H. (1994). A new type of defect in the gene for bilirubin uridine 5'-diphosphate-glucuronosyltransferase in a patient with Crigler-Najjar syndrome type I. Pediatr. Res. *35*, 629–632. https://doi.org/10.1203/00006450-199406000-00002.

Bassari, R., and Koea, J.B. (2015). Jaundice associated pruritis: a review of pathophysiology and treatment. World J. Gastroenterol. *21*, 1404–1413. https://doi.org/10.3748/wjg.v21.i5.1404.

Bhasin, S., Sikka, S., Fielder, T., Sod-Moriah, U., Levine, H.B., Swerdloff, R.S., and Rajfer, J. (1986). Hormonal effects of ketoconazole in vivo in the male rat: mechanism of action. Endocrinology *118*, 1229–1232. https://doi.org/10.1210/endo-118-3-1229.

Bortolussi, G., and Muro, A.F. (2020). Experimental models assessing bilirubin neurotoxicity. Pediatr. Res. *87*, 17–25. https://doi.org/10.1038/s41390-019-0570-x.

Chen, Y., Li, Y., Wang, X., Zhang, W., Sauer, V., Chang, C.-J., Han, B., Tchaikovskaya, T., Avsar, Y., Tafaleng, E., et al. (2015). Amelioration of Hyperbilirubinemia in Gunn Rats after Transplantation of Human Induced Pluripotent Stem Cell-Derived Hepatocytes. Stem Cell Rep. *5*, 22–30. https://doi.org/10.1016/j.stemcr.2015.04.017.

Collaud, F., Bortolussi, G., Guianvarc'h, L., Aronson, S.J., Bordet, T., Veron, P., Charles, S., Vidal, P., Sola, M.S., Rundwasser, S., et al. (2019). Preclinical Development of an AAV8-hUGT1A1 Vector for the Treatment of Crigler-Najjar Syndrome. Mol. Ther. Methods Clin. Dev. *12*, 157–174. https://doi.org/10.1016/j.omtm.2018.12.011.

Cui, J., Pan, Y.H., Zhang, Y., Jones, G., and Zhang, S. (2011). Progressive pseudogenization: vitamin C synthesis and its loss in bats. Mol. Biol. Evol. *28*, 1025–1031. https://doi.org/10.1093/molbev/msq286.

Fourrier, A., Delbos, F., Menoret, S., Collet, C., Thi Thuy, L.T., Myara, A., Petit, F., Tolosa, L., Laplanche, S., Gómez-Lechón, M.J., et al. (2020). Regenerative cell therapy for the treatment of hyperbilirubinemic Gunn rats with fresh and frozen human induced pluripotent stem cells-derived hepatic stem cells. Xenotransplantation *27*, e12544. https://doi.org/10.1111/xen.12544.

Gao, Y., Zhang, X., Zhang, L., Cen, J., Ni, X., Liao, X., Yang, C., Li, Y., Chen, X., Zhang, Z., et al. (2017). Distinct Gene Expression and Epigenetic Signatures in Hepatocyte-like Cells Produced by Different Strategies from the Same Donor. Stem Cell Rep. *9*, 1813–1824. https://doi.org/10.1016/j.stemcr.2017.10.019.

Gottimukkala, S.B., Lobo, L., Gautham, K.S., Bolisetty, S., Fiander, M., and Schindler, T. (2023). Intermittent phototherapy versus continuous phototherapy for neonatal jaundice. Cochrane Database Syst. Rev. *3*, CD008168. https://doi.org/10.1002/14651858.CD008168.pub2.

Hoekstra, R., Nibourg, G.A.A., van der Hoeven, T.V., Plomer, G., Seppen, J., Ackermans, M.T., Camus, S., Kulik, W., van Gulik, T.M., Elferink, R.P.O., and Chamuleau, R.A.F.M. (2013). Phase 1 and phase 2 drug metabolism and bile acid production of HepaRG cells in a bioartificial liver in absence of dimethyl

sulfoxide. Drug Metab. Dispos. *41*, 562–567. https://doi.org/10.1124/dmd.112.049098.

Kammerer, S., and Küpper, J.H. (2018). Human hepatocyte systems for in vitro toxicology analysis. J. Cell. Biotechnol. *3*, 85–93. https://doi.org/10.3233/JCB-179012.

Khadem al-hosseini, M., Rahideh, S.T., Saadati, A., Rahmati, N., Azadeh, F., Janani, L., and Shidfar, F. (2020). The effect of vitamin C supplementation in the last month of pregnancy on neonatal bilirubin levels; A double-blind randomized clinical trial. Compl. Ther. Med. *50*, 102359. https://doi.org/10.1016/j.ctim.2020.102359.

Khor, T.O., Fuentes, F., Shu, L., Paredes-Gonzalez, X., Yang, A.Y., Liu, Y., Smiraglia, D.J., Yegnasubramanian, S., Nelson, W.G., and Kong, A.-N.T. (2014). Epigenetic DNA Methylation of Antioxidative Stress Regulator NRF2 in Human Prostate Cancer. Cancer Prev. Res. *7*, 1186–1197. https://doi.org/10.1158/1940-6207.Capr-14-0127.

Kim, B.H., Joo, Y., Kim, M.S., Choe, H.K., Tong, Q., and Kwon, O. (2021). Effects of Intermittent Fasting on the Circulating Levels and Circadian Rhythms of Hormones. Endocrinol. Metab. *36*, 745–756. https://doi.org/10.3803/EnM.2021.405.

Kim, S.R., Ha, Y.M., Kim, Y.M., Park, E.J., Kim, J.W., Park, S.W., Kim, H.J., Chung, H.T., and Chang, K.C. (2015). Ascorbic acid reduces HMGB1 secretion in lipopolysaccharide-activated RAW 264.7 cells and improves survival rate in septic mice by activation of Nrf2/HO-1 signals. Biochem. Pharmacol. *95*, 279–289. https://doi.org/10.1016/j.bcp.2015.04.007.

Kimura, M., Iguchi, T., Iwasawa, K., Dunn, A., Thompson, W.L., Yoneyama, Y., Chaturvedi, P., Zorn, A.M., Wintzinger, M., Quattrocelli, M., et al. (2022). En masse organoid phenotyping informs metabolic-associated genetic susceptibility to NASH. Cell *185*, 4216–4232.e16.

Kobayashi, T., Takeba, Y., Ohta, Y., Ootaki, M., Kida, K., Watanabe, M., Iiri, T., and Matsumoto, N. (2022). Prenatal glucocorticoid administration enhances bilirubin metabolic capacity and increases Ugt1a and Abcc2 gene expression via glucocorticoid receptor and PXR in rat fetal liver. J. Obstet. Gynaecol. Res. *48*, 1591–1606. https://doi.org/10.1111/jog.15235.

Kumagai, A., Ando, R., Miyatake, H., Greimel, P., Kobayashi, T., Hirabayashi, Y., Shimogori, T., and Miyawaki, A. (2013). A Bilirubin-Inducible Fluorescent Protein from Eel Muscle. Cell *153*, 1602–1611. https://doi.org/10.1016/j.cell.2013.05.038.

Kumar, R.K. (1999). Neonatal jaundice. An update for family physicians. Aust. Fam. Physician *28*, 679–682.

Le Pichon, J.B., Riordan, S.M., Watchko, J., and Shapiro, S.M. (2017). The Neurological Sequelae of Neonatal Hyperbilirubinemia: Definitions, Diagnosis and Treatment of the Kernicterus Spectrum Disorders (KSDs). Curr. Pediatr. Rev. *13*, 199–209. https://doi.org/10.2174/1573396313666170815100214.

Maerckx, C., Tondreau, T., Berardis, S., van Pelt, J., Najimi, M., and Sokal, E. (2014). Human liver stem/progenitor cells decrease serum bilirubin in hyperbilirubinemic Gunn rat. World J. Gastroenterol. *20*, 10553–10563. https://doi.org/10.3748/wjg.v20.i30.10553.

Martin, H. (2010). Role of PPAR-gamma in inflammation. Prospects for therapeutic intervention by food components. Mutat. Res. *690*, 57–63. https://doi.org/10.1016/j.mrfmmm.2009.09.009.

Mitsuishi, Y., Motohashi, H., and Yamamoto, M. (2012). The Keap1–Nrf2 system in cancers: stress response and anabolic metabolism. Front. Oncol. *2*, 200. https://doi.org/10.3389/fonc.2012.00200.

Mostafavi-Pour, Z., Ramezani, F., Keshavarzi, F., and Samadi, N. (2017). The role of quercetin and vitamin C in Nrf2-dependent oxidative stress production in breast cancer cells. Oncol. Lett. *13*, 1965–1973. https://doi.org/10.3892/ol.2017.5619.

Olusanya, B.O., Teeple, S., and Kassebaum, N.J. (2018). The Contribution of Neonatal Jaundice to Global Child Mortality: Findings From the GBD 2016 Study. J Pediatrics *141*, e20171471. https://doi.org/10.1542/peds.2017-1471.

Ouchi, R., Togo, S., Kimura, M., Shinozawa, T., Koido, M., Koike, H., Thompson, W., Karns, R.A., Mayhew, C.N., McGrath, P.S., et al. (2019). Modeling Steatohepatitis in Humans with Pluripotent Stem Cell-Derived Organoids. Cell Metab. *30*, 374–384.e6. https://doi.org/10.1016/j.cmet.2019.05.007.

Pall, M.L., and Levine, S. (2015). Nrf2, a master regulator of detoxification and also antioxidant, anti-inflammatory and other cytoprotective mechanisms, is raised by health promoting factors. Sheng Li Xue Bao *67*, 1–18.

Peterson, E.A., Polgar, Z., Devakanmalai, G.S., Li, Y., Jaber, F.L., Zhang, W., Wang, X., Iqbal, N.J., Murray, J.W., Roy-Chowdhury, N., et al. (2019). Genes and Pathways Promoting Long-Term Liver Repopulation by Ex Vivo hYAP-ERT2 Transduced Hepatocytes and Treatment of Jaundice in Gunn Rats. Hepatol. Commun. *3*, 129–146. https://doi.org/10.1002/hep4.1278.

Pundir, S., Gridneva, Z., Pillai, A., Thorstensen, E.B., Wall, C.R., Geddes, D.T., and Cameron-Smith, D. (2020). Human Milk Glucocorticoid Levels Are Associated With Infant Adiposity and Head Circumference Over the First Year of Life. Front. Nutr. *7*, 166. https://doi.org/10.3389/fnut.2020.00166.

Relling, M.V., Nemec, J., Schuetz, E.G., Schuetz, J.D., Gonzalez, F.J., and Korzekwa, K.R. (1994). O-demethylation of epipodophyllotoxins is catalyzed by human cytochrome P450 3A4. Mol. Pharmacol. *45*, 352–358.

Sai, K., Lal, A., Lakshmi Maradana, J., Velamala, P.R., and Nitin, T. (2019). Hypokalemia associated with mifepristone use in the treatment of Cushing's syndrome. Endocrinol. Diabetes Metab. Case Rep. *2019*, 19-0064. https://doi.org/10.1530/edm-19-0064.

Savini, I., Rossi, A., Pierro, C., Avigliano, L., and Catani, M.V. (2008). SVCT1 and SVCT2: key proteins for vitamin C uptake. Amino Acids *34*, 347–355. https://doi.org/10.1007/s00726-007-0555-7.

Sharma, D., Bhave, S., Gregg, E., and Uht, R. (2013). Dexamethasone induces a putative repressor complex and chromatin modifications in the CRH promoter. Mol. Endocrinol. *27*, 1142–1152. https://doi.org/10.1210/me.2013-1079.

Shinozawa, T., Kimura, M., Cai, Y., Saiki, N., Yoneyama, Y., Ouchi, R., Koike, H., Maezawa, M., Zhang, R.R., Dunn, A., et al. (2021). High-Fidelity Drug-Induced Liver Injury Screen Using Human Pluripotent Stem Cell-Derived Organoids. Gastroenterology *160*, 831–846.e10. https://doi.org/10.1053/j.gastro.2020.10.002.

Sugatani, J., Nishitani, S., Yamakawa, K., Yoshinari, K., Sueyoshi, T., Negishi, M., and Miwa, M. (2005). Transcriptional regulation of

human UGT1A1 gene expression: activated glucocorticoid receptor enhances constitutive androstane receptor/pregnane X receptor-mediated UDP-glucuronosyltransferase 1A1 regulation with glucocorticoid receptor-interacting protein 1. Mol. Pharmacol. *67*, 845–855. https://doi.org/10.1124/mol.104.007161.

Tcaciuc, E., Podurean, M., and Tcaciuc, A. (2021). Management of Crigler-Najjar syndrome. Med. Pharm. Rep. *94*. S64-s67. https://doi.org/10.15386/mpr-2234.

Theiler-Schwetz, V., Schlager, H., Obermayer-Pietsch, B., Stojakovic, T., Fauler, G., Fickert, P., and Zollner, G. (2021). Hypercortisolism in patients with cholestasis is associated with disease severity. BMC Gastroenterol. *21*, 460. https://doi.org/10.1186/s12876-021-02045-4.

van de Steeg, E., van Esch, A., Wagenaar, E., Kenworthy, K.E., and Schinkel, A.H. (2013). Influence of Human OATP1B1, OATP1B3, and OATP1A2 on the Pharmacokinetics of Methotrexate and Paclitaxel in Humanized Transgenic Mice. Clin. Cancer Res. *19*, 821–832. https://doi.org/10.1158/1078-0432.CCR-12-2080.

Watson, R.L. (2009). Hyperbilirubinemia. Crit. Care Nurs. Clin. North Am. *21*, 97–120. https://doi.org/10.1016/j.ccell.2008.11.001.

Werumeus Buning, J., Kootstra-Ros, J.E., Brummelman, P., van den Berg, G., van der Klauw, M., Wolffenbuttel, B.H.R., Van Beek, A.P., and Dullaart, R.P.F. (2016). Higher hydrocortisone dose increases bilirubin in hypopituitary patients- Results from an RCT. Eur. J. Clin. Invest. *46*, 475–480. https://doi.org/10.1111/eci.12624.

Xu, L.-L., Zhao, B., Sun, S.-L., Yu, S.-F., Wang, Y.-M., Ji, R., Yang, Z.-T., Ma, L., Yao, Y., Chen, Y., et al. (2020). High-dose vitamin C alleviates pancreatic injury via the NRF2/NQO1/HO-1 pathway in a rat model of severe acute pancreatitis. Ann. Transl. Med. *8*, 852.

Yueh, M.F., and Tukey, R.H. (2007). Nrf2-Keap1 signaling pathway regulates human UGT1A1 expression in vitro and in transgenic UGT1 mice. J. Biol. Chem. *282*, 8749–8758. https://doi.org/10.1074/jbc.M610790200.

Zhang, W., He, Y.J., Gan, Z., Fan, L., Li, Q., Wang, A., Liu, Z.Q., Deng, S., Huang, Y.F., Xu, L.Y., and Zhou, H.H. (2007). OATP1B1 polymorphism is a major determinant of serum bilirubin level but not associated with rifampicin-mediated bilirubin elevation. Clin. Exp. Pharmacol. Physiol. *34*, 1240–1244. https://doi.org/10.1111/j.1440-1681.2007.04798.x.

Stem Cell Reports, Volume *18*

Supplemental Information

Synthetic augmentation of bilirubin metabolism in human pluripotent stem cell-derived liver organoids

Hasan Al Reza, Zishaan Farooqui, Abid Al Reza, Callen Conroy, Kentaro Iwasawa, Yasuhiro Ogura, Keisuke Okita, Kenji Osafune, and Takanori Takebe

Supplementary data related to manuscript:

Synthetic Augmentation of Bilirubin Metabolism in Human Pluripotent Stem Cell-derived Liver Organoids

Reza HA *et al.*, 2023

Overview

Supplementary Figures and Legends

Figure S1. Development and characterization of HLOs from healthy iPSC. Related to Figure 1.

Figure S2. Further development and characterization of HLOs from all cell lines. Related to Figure 1.

Figure S3. Effect of Dexamethasone and Mifepristone on HLOs. Related to Figure 2-3.

Figure S4. Characterization of mGULO iPSC and eHLO. Related to Figure 4.

Figure S5. Orthotropic transplantation of HLOs improve overall liver health. Related to Figure 5.

Supplementary Tables

Table S1: List of antibodies used for immunostaining (IC), ELISA, ChIP-qPCR (ChIP) and organoid experiment. Related to all figures.

Table S2: List of TaqMan probes used for qPCR. Related to all figures.

Table S3: List of Custom primers used for ChIP-qPCR. Related to Figure 2.

Supplementary Figures and Legends

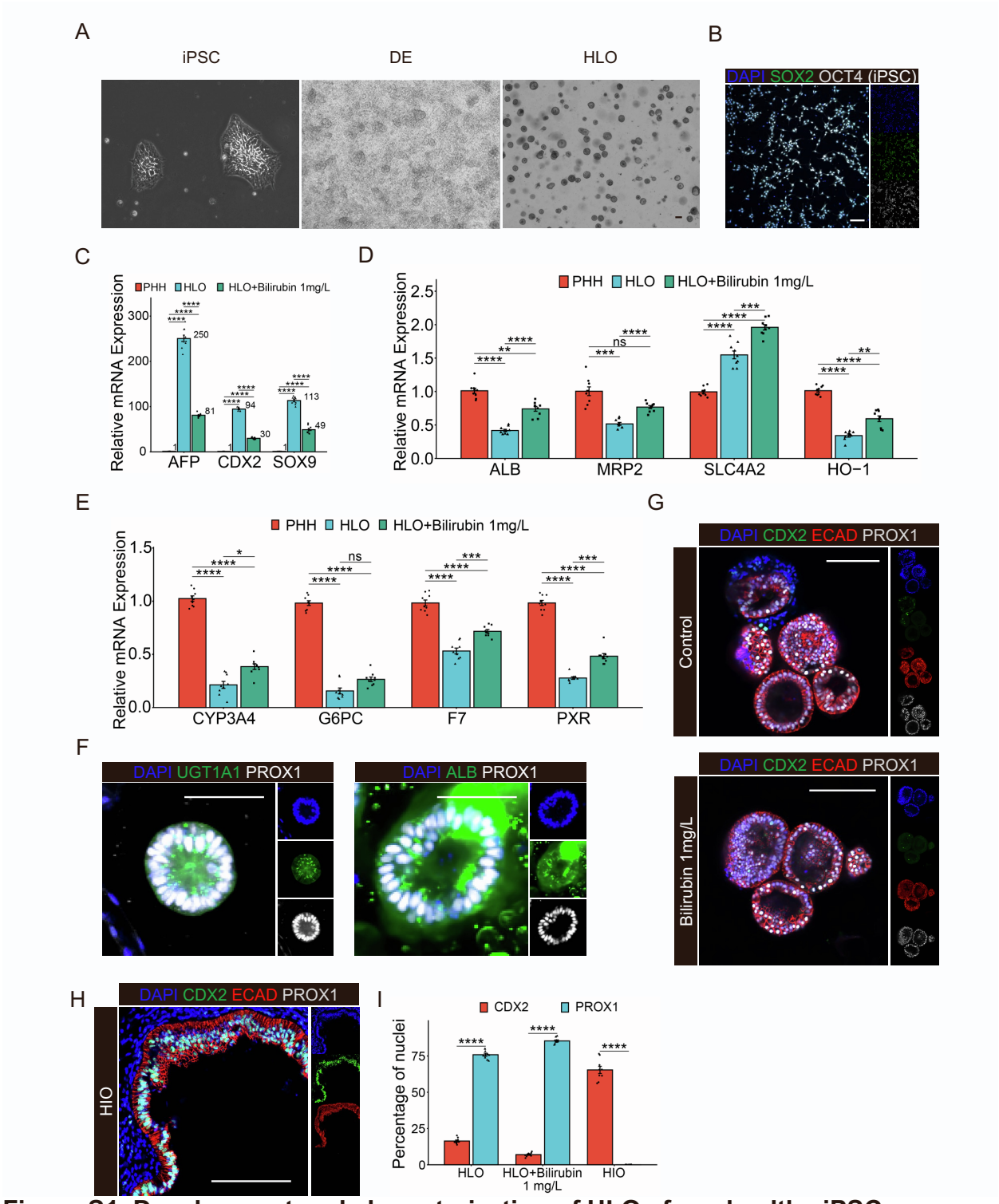

Figure S1. Development and characterization of HLOs from healthy iPSC.

A) Brightfield image of healthy iPSCs, Definitive Endoderm, and HLOs. Scale bar indicates 200 µm.

B) Immunofluorescence images of healthy iPSCs depicting pluripotent markers such as SOX2 and OCT4. Scale bar indicates 200 μm.
C) RT-qPCR of *AFP* and *CDX2* gene for HLOs primed with bilirubin compared to control HLOs and PHH. (Data is mean ± SD, n = 9 independent experiments)
D) RT-qPCR of *ALB, NANOG, SLC4A2,* and *HO-1* gene for HLOs primed with bilirubin compared to control HLOs and PHH. (Data is mean ± SD, n = 9 independent experiments)
E) RT-qPCR of *CYP3A4, G6PC, F7,* and *PXR* gene for HLOs primed with bilirubin compared to control HLOs and PHH. (Data is mean ± SD, n = 9 independent experiments)
F) Immunofluorescence images of healthy HLOs for UGT1A1, ALB, and PROX1. Scale bar indicates 200 μm.
G) Immunofluorescence images for CDX2, PROX1, and ECAD of bilirubin primed HLOs compared to control. Scale bar indicates 200 μm.
H) Immunofluorescence images for CDX2, PROX1, and ECAD of HIOs. Scale bar indicates 200 μm.
I) Quantitation of CDX2+ and PROX1+ nuclei in bilirubin primed HLOs compared to control.

A

CNS patient profile	
Ethnicity	Japanese
Disease	CNS Type 1, Jaundice (Total Bili: 20mg/dL), growth retardation
Treatment	Non-responsive to phototherapy, phenobarbital
Mutation	UGT1A1 exon1 point mutation

B

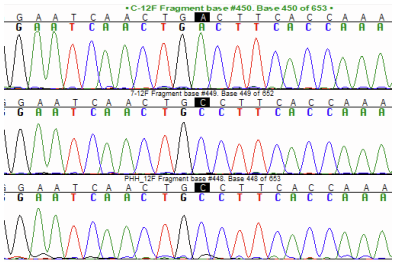

C

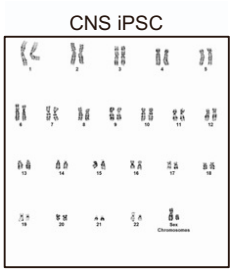

D

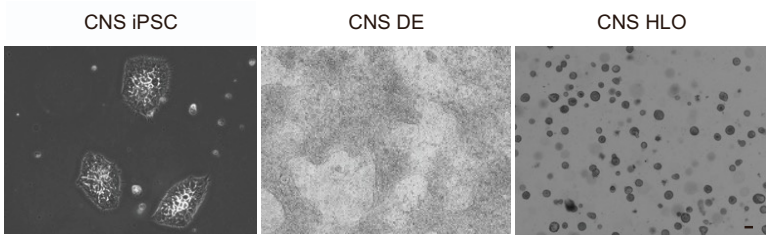

E

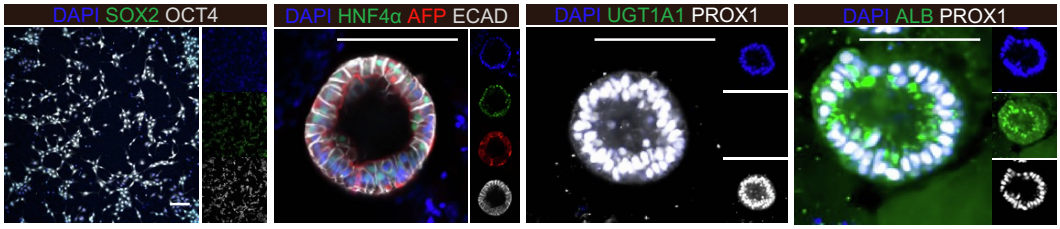

F

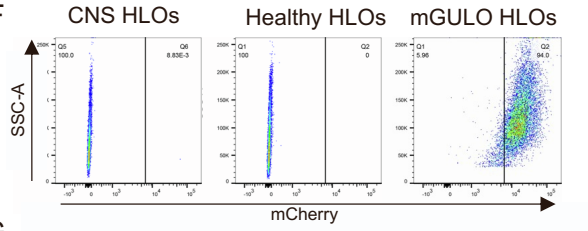

G

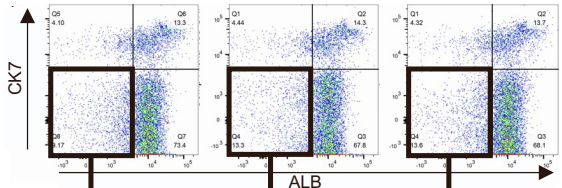

H

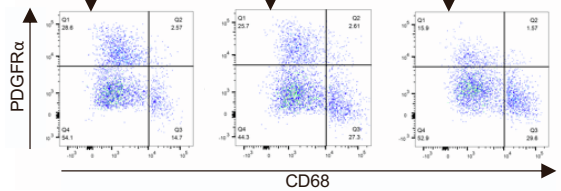

I

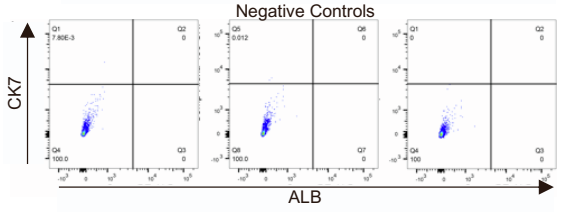

J

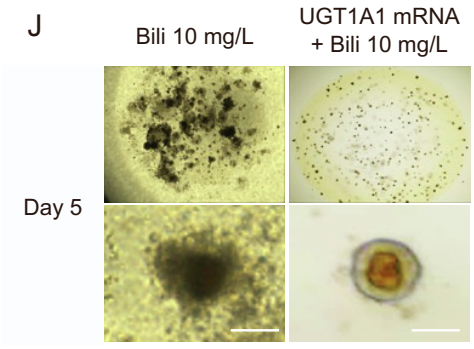

K

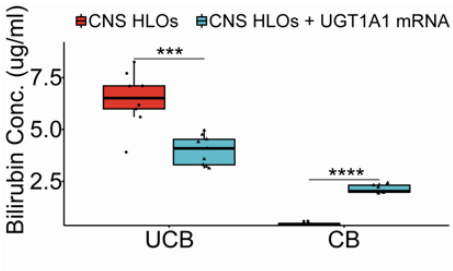

Figure S2. Further development and characterization of HLOs from all cell lines.

A) Patient details for the person from which the CNS iPSC was derived from.
B) Sanger sequencing depicting a c.858C>A (p.Cys280X) nonsense mutation in CNS iPSC compared to healthy iPSC and PHH.
C) Karyotype analysis of CNS iPSC line: standard metaphase spreads and G-banded karyotype were processed and interpreted by the CCHMC cytogenetics core.
D) Brightfield image of CNS iPSCs, Definitive Endoderm, and HLOs. Scale bar indicates 200 μm.
E) Immunofluorescence images of CNS iPSCs depicting pluripotent markers such as SOX2 and OCT4. The CNS HLOS express HNF4α, UGT1A1, ALB, PROX1, and AFP. Scale bar indicates 200 μm.
F) CNS iPSC, Healthy iPSC, and mGULO iPSC derived HLOs exhibit similar cellular diversity. Only mGULO HLOs exhibit 94% mCherry+ cells.
G) CNS HLOs, Healthy HLOs, and mGULO HLOs have 86.7, 82, and 81.7% ALB+ cells respectively indicating hepatocytes while 17.4, 18.8 and 18.1% CK7+ cells respectively were observed which were cholangiocyte like cells. Additionally, there was an ALB+ CK7+ (dual positive population) that were hepatoblast like cells in all 3 organoid lines (13.3, 14.3 and 13.7% in CNS HLOs, Healthy HLOs, and mGULO HLOs respectively).
H) Finally, 2.62, 3.42, and 2.16% (28.6, 25.7, and 15.9% of ALB- CK7-) PDGFRα+ stellate like cells and 1.35, 3.63, and 4.03% (14.7, 27.3, and 29.6% of ALB- CK7-) CD68 expressing macrophage like cells were observed in CNS HLOs, Healthy HLOs, and mGULO HLOs respectively.
I) Negative controls have almost 0% of ALB+ and CK7+ cells.
J) Brightfield image of CNS HLOs transfected with UGT1A1 mRNA compared to control after treatment with bilirubin (10 mg/L).
K) Bilirubin assay measuring unconjugated and conjugated bilirubin in CNS HLOs transfected with UGT1A1 mRNA compared to control. (n = 9 independent experiments)

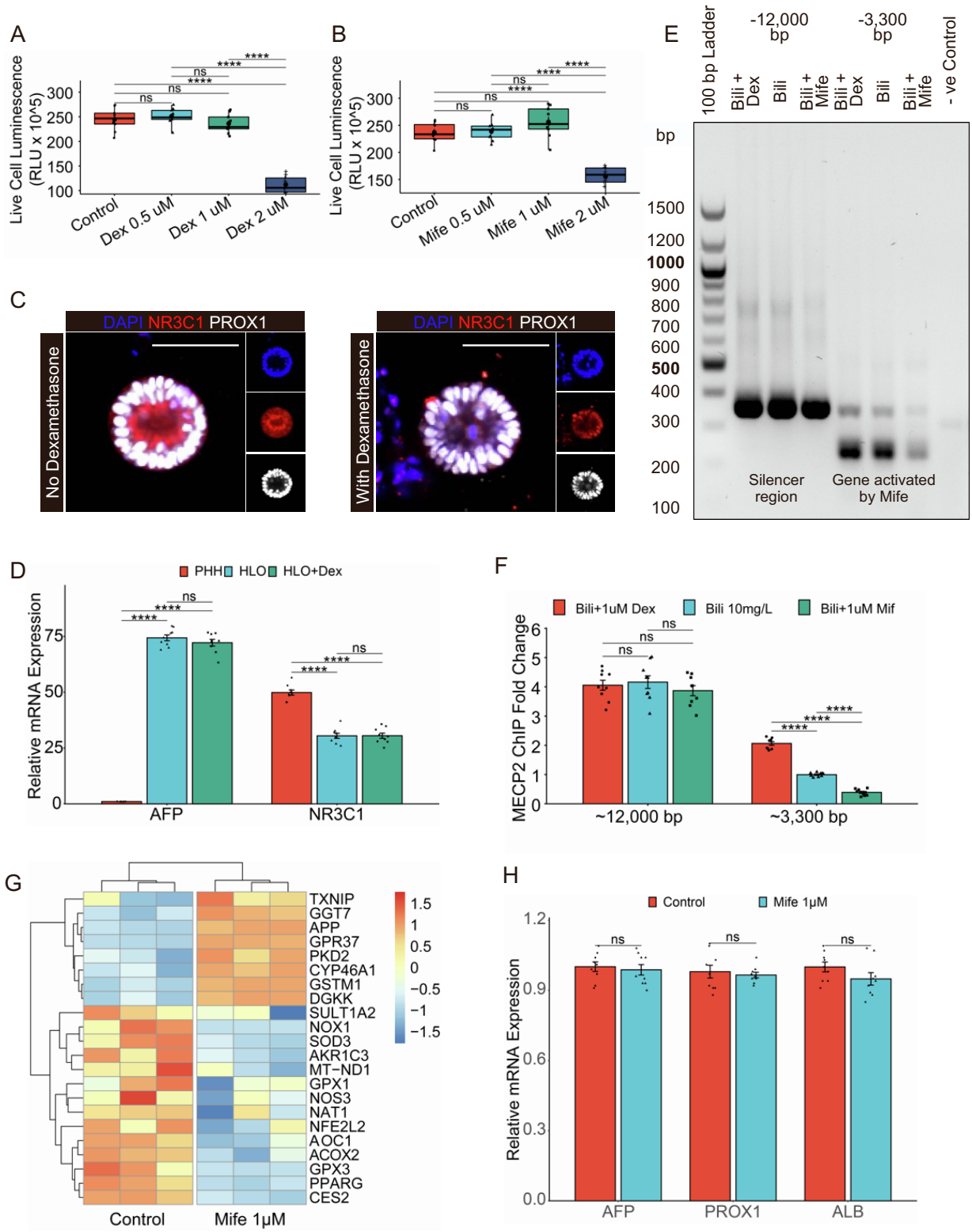

Figure S3. Effect of Dexamethasone and Mifepristone on HLOs.

A) Cell Viability Assay on HLOs treated with different concentration of Dexamethasone.

B) Cell Viability Assay on HLOs treated with different concentration of Mifepristone.

C) Immunofluorescence images for NR3C1, and PROX1of dexamethasone treated

HLOs compared to control. Scale bar indicates 200 μm.

D) RT-qPCR of *NR3C1* and *AFP* gene for HLOs treated with Dexamethasone compared to control and PHH. (Data is mean ± SD, n = 9 independent experiments)

E) MECP2 ChIP-PCR for organoids treated with 10mg/L Bilirubin and Mifepristone (1 uM) or Dexamethasone (1 uM).

F) MECP2 ChIP-qPCR for samples in (F). (Data is mean ± SD, n = 9 independent experiments)

G) Heatmap for genes important for both Xenobiotic and ROS metabolism in Mifepristone treated organoids compared to control after treatment with bilirubin.

H) RT-qPCR of *ALB, PROX1,* and *AFP* gene for Mifepristone treated organoids compared to control after treatment with bilirubin. (Data is mean ± SD, n = 9 independent experiments)

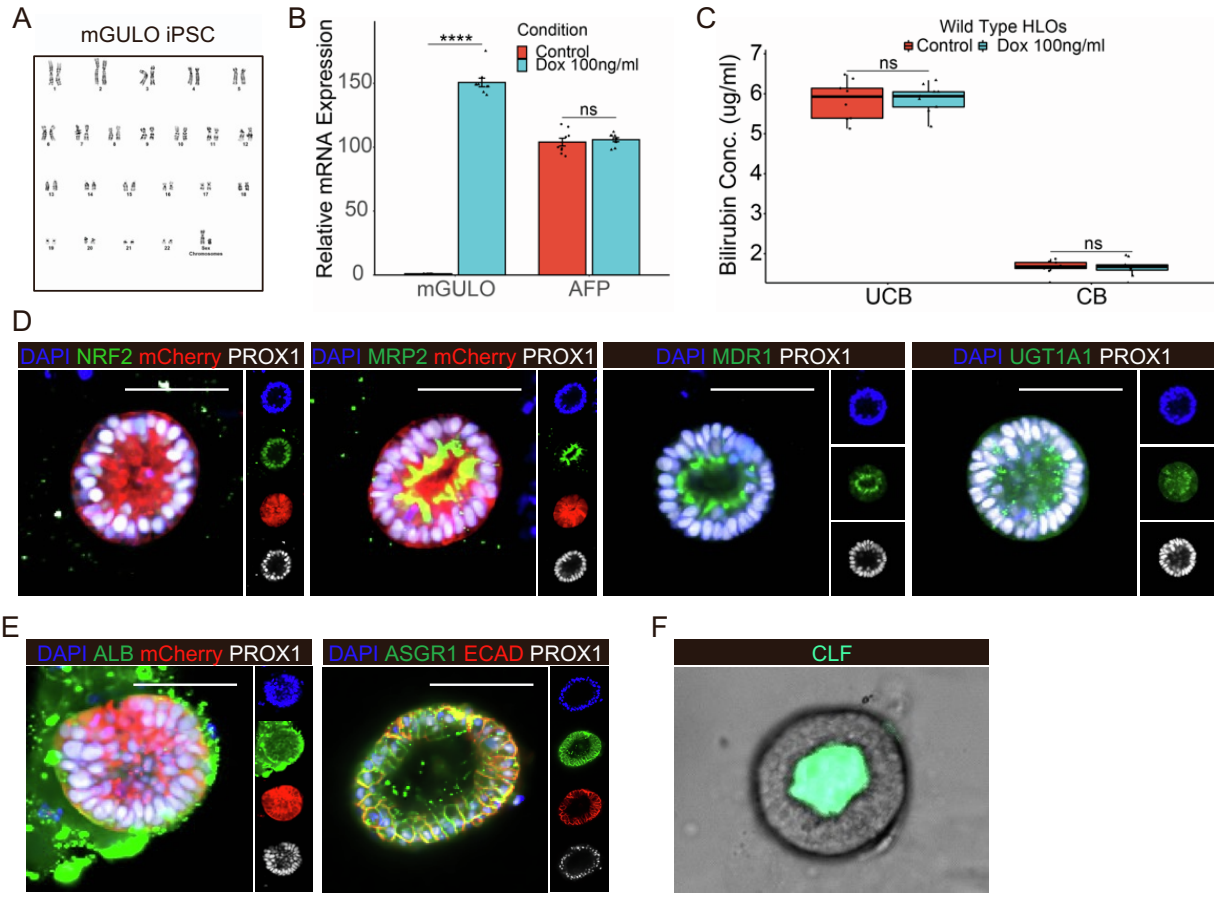

Figure S4. Characterization of mGULO iPSC and eHLO.

A) Karyotype analysis of mGULO iPSC line: standard metaphase spreads and G-banded karyotype were processed and interpreted by the CCHMC cytogenetics core.

B) RT-qPCR of *mGULO* and *AFP* gene for mGULO organoids treated with Dox (100 ng/ml) compared to control. (Data is mean ± SD, n = 9 independent experiments)

C) Bilirubin assay measuring unconjugated and conjugated bilirubin in wild type HLOs treated with bilirubin (10 mg/L) and Dox (100 ng/ml) compared to control. (n = 9 independent experiments)

D) Immunofluorescence images for NRF2, mCherry, MRP2, MDR1, UGT1A1, and PROX1 in eHLOs. Scale bar indicates 200 μm.

E) Immunofluorescence images for mCherry, ALB, PROX1, ASGR1, and ECAD in eHLOs. Scale bar indicates 200 μm.

F) Fluorescent bile acid (CLF, green) uptake assay in eHLOs. Scale bar indicates 200 μm.

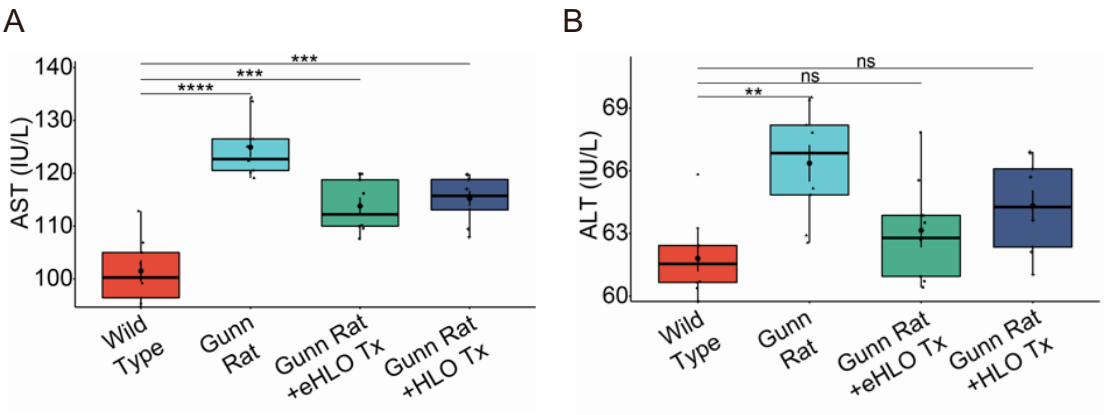

Figure S5. Orthotropic transplantation of HLOs improve overall liver health.

A) AST assay on Gunn rats after transplantation compared to sham and wild type rats. (n = 9 independent experiments)

B) ALT assay on Gunn rats after transplantation compared to sham and wild type rats. (n = 9 independent experiments)

Table S1: List of antibodies used for immunostaining (IC), ELISA, ChIP-qPCR (ChIP) and organoid experiment.

Antibody	Host	Source	Catalog #	Dilution	Method
MeCP2 ChIP Grade	Rabbit	abcam	ab2828	5μg	ChIP
HNF4α	Rabbit	abcam	ab201460	1:200	IF
AFP	Mouse	eBioscience	14-9499	1:200	IF
CDH1	Goat	R&D	AF648	1:200	IF
GCR	Rabbit	Invitrogen	PA1-511A	1:200	IF
SLCO1B1	Mouse	Novus	NB100-74482	1:200	IF
NCOR	Rabbit	abcam	ab24552	1:200	IF
MRP2	Mouse	Novus	NB110-6000	1:100	IF
SOX2	Goat	R&D	AF2018	1:200	IF
OCT4	Mouse	Santa cruz	sc-5279	1:200	IF
UGT1A1	Mouse	Santa cruz	sc-271268	1:200	IF
PROX1	Goat	R&D	AF2727	1:200	IF
CDX2	Rabbit	Bethyl	A300-691A	1:200	IF
CDH1	Mouse	Thermo	334000	1:200	IF
NR3C1	Rabbit	Abcam	ab24552	1:200	IF, ChIP
NRF2	Rabbit	Abcam	ab31163	1:200	IF
MRP2	Mouse	Novus	NB110-6000	1:200	IF
MDR1	Rabbit	Bioss	BS-0563R	1:200	IF
ALB	Mouse	R&D	MAB1455	1:200	IF
ALB	Goat	Bethyl	A80-129A	1μg	ELISA
ALB-PE	Mouse	Novus	IC1455P	1:200	Flow cytometry
CK7- Alexa Fluor 488	Rabbit	Abcam	ab185048	1:200	Flow cytometry
PDGFRα-BV711	Mouse	BD Bioscience	752901	1:200	Flow cytometry
CD68-APC	Mouse	R&D	IC20401A	1:200	Flow cytometry
normal IgG control	Rabbit	abcam	ab37415	5μg	ChIP

Table S2: List of TaqMan probes used for qPCR

Gene	Gene name	TaqMan probe (Catalog #)
UGT1A1	UDP-glucuronosyltransferase 1A1	Hs02511055_s1
NRF2	Nuclear factor erythroid 2-related factor 2	Hs00975961_g1
IL-6	Interleukin 6	Hs00174131_m1
mGULO	Murine L-Gulonolactone oxidase	Mm00626646_m1
AFP	Alpha-fetoprotein	HS01040598_m1
CDX2	Caudal type homeobox 2	Hs01078080_m1
SOX9	SRY-box transcription factor 9	Hs00165814_m1
ALB	Albumin	Hs00609411_m1
MRP2	ATP binding cassette subfamily C member 2	Hs00166123_m1
SLC4A2	Solute carrier family 4 member 2	Hs01586776_m1
HO-1	Heme oxygenase 1	Hs01110250_m1
CYP3A4	Cytochrome P450 family 3 subfamily A member 4	Hs00604506_m1
G6PC	Glucose-6-phosphatase	Hs00609178_m1
F7	Coagulation factor VII	Hs01551994_m1
PXR	Nuclear receptor subfamily 1 group I member 2	Hs01114267_m1

Table S3: List of Custom primers used for ChIP-qPCR

Orientation	Sequence
Forward *UGT1A1* XRE	AAGGTCACTCAATTCCAAGGG
Probe *UGT1A1* XRE	/56-FAM/AGGGTATTA/ZEN/GGTGTAATGAGGATGTGT/3IABkFQ/
Reverse *UGT1A1* XRE	CTCAGAAGTTTGTTCTGGTGAGA
Forward *UGT1A1* Silencer	CCTGCTGGTCTCATCATAGTG
Probe *UGT1A1* Silencer	GAAAGTGAGAGAGAGGCAAAGA
Reverse *UGT1A1* Silencer	/56-FAM/TCCCTTCAC/ZEN/TTGCAAGCTCTTCCT/3IABkFQ/

Supplementary Experimental Procedures

CNS and mGULO iPSC generation and general iPSCs maintenance

Experiments using iPSCs were approved by the Ethics Committees of Cincinnati Children's Hospital Medical Center and Kyoto University. A CNS patient from whom iPSCs were derived provided written informed consent. The iPSC lines were generated from the patient as previously reported (Okita et al., 2011; Okita et al., 2013). Briefly, peripheral blood mononuclear cells (PBMCs) were obtained from the patient at the Kyoto University Hospital and cultured in StemSpan-ACF (STEMCELL Technologies) supplemented with 100 ng/mL IL-6, 300 ng/mL SCF, 300 ng/mL TPO, 300 ng/mL Flt3 ligand, 10 ng/mL IL-3 (PeproTech) for 6 days. The cells were reprogrammed by introducing pCXLE-hOCT3/4-shp53-F, pCXLE-hSK, pCXLE-hUL, and pCXWB-EBNA1, which encoded OCT3/4, SOX2, KLF4, L-MYC, LIN28, and shRNA against TP53 under on feeder culture conditions. The 1383D6 and RCL-BC iPSC used in this study was kindly provided by CiRA, Kyoto University and RxCell Inc. respectively. CuSTOM1 iPSC was obtained from patient foreskin fibroblasts and reprogrammed into iPSC by Cincinnati Children’s Hospital Medical Center pluripotent stem cell core (Pitstick et al., 2022). The PCSF#117 vector with the modified GULO sequence was then inserted into the AAVS1 locus of the CuSTOM1 iPSC cell line using a lentiviral mediated CRISPR/Cas9. The correct clones were then selected using G418. The surviving clones were then verified for correct insertion, random insertion and copy number using PCR, and verified by DNA sequencing. The iPSCs were then maintained on Laminin iMatrix-511 Silk (REPROCELL USA Inc.) coated cell culture plates and maintained with StemFit Basic04 Complete Type

(Ajinomoto Company) media with Y-27632 (Stem Cell Technologies). The cells were passaged every 7 days with Accutase (Sigma-Aldrich) until passage 40 (p40).

Organoid generation

The p40 cells were plated on a 24 well plate coated with Laminin iMatrix-511 Silk at a density of 2X10^5 cells/well and maintained with Stemfit media with 10 μM Y-27632. On Day 2, the media was replaced with fresh Stemfit. The following day, the cells were treated with RPMI 1640 (Gibco) media mixed with 100 ng/ml Activin A (Shenandoah Biotechnology) and 50 ng/ml BMP4 (R&D Systems) to generate definitive endoderm. On the 4th day, the media was replaced with RPMI, 100 ng/ml Activin A and 0.2% dFBS (HyClone) which was changed to 2% dFBS on day 5. From Day 6-8, the cells were fed with 500 ng/ml FGF-4 (Shenandoah Biotechnology) and 3 μM CHIR99021 (PeproTech) in Adv. DMEM [Advanced DMEM/F-12 (Gibco) with B27 (Gibco), N2 (Gibco), 10mM HEPES (Gibco), 2 mM L-glutamine (Gibco), and GA-1000 (Lonza)] to induce posterior foregut. On Day 9, the cells were dissociated into a single cell suspension using Accutase treatment. This single cell suspension was then mixed with 50% Matrigel (Corning Cat# 356237) and 50% EP media and plated as 50 ul drops in a 6-well plate. These cells were fed with EP media every 48 hrs for 4 days to generate organoids. These organoids were then treated with Adv. DMEM and 2 μM RA (Sigma-Aldrich) every 48 hrs for 4 days to specify the hepatic lineage. The organoids were then filtered through a 160 μm mesh filter and fed with HCM (Lonza), 10 ng/ml HGF (PeproTech), 20 ng/ml Oncostatin M (PeproTech) and 0.1 μM Dexamethasone (Sigma-Aldrich) every 3-4 days to generate

HLOs and passaged as necessary by passing them through a 160 μm mesh filter to maintain consistency of HLO and mesenchyme ratio.

Flow cytometry

For flow cytometry, the organoids were dissociated from the Matrigel on Day 27 by pipetting and washed. The organoids were then dissociated into single cells using 10% 10X TrypLE Select Enzyme (Gibco, A1217701) and 90% Trypsin-EDTA (Gibco, 25200056) and centrifuged at 1500 rpm for 3 minutes. Each cell pellet was washed with 1x PBS (Gibco, 14190235), strained using a 100μm strainer (Falcon, 08-771-19) and counted using a hemocytometer before being stained using the Transcription Factor Buffer Set (BD Pharmingen, 562574) according to the manufacturer's instructions. Stained or unstained controls were included. Subsequently, the unstained or stained cells were washed at room temperature and pelleted. The pellet was then resuspended in Stain Buffer (FBS) (BD Pharmingen, 554656) and filtered into FACS tubes. Flow cytometry run was performed using BD LSR Fortessa X20 with UltraComp eBeads Compensation Beads (Invitrogen, 01-2222-41) and finally, the flow cytometry data was analyzed using FlowJo.

RNA extraction, RT-qPCR, and RNA sequencing

RNA was isolated using the RNeasy mini kit (Qiagen, Hilden, Germany). Reverse transcription was carried out using the High-Capacity cDNA Reverse Transcription Kit for RT-PCR (Applied Biosystems) according to manufacturer's protocol. qPCR was carried out using TaqMan gene expression master mix (Applied Biosystems) on a QuantStudio

5 Real-Time PCR System (Applied Biosystems). All the samples were amplified with TaqMan Gene Expression Assays and normalized with 18S rRNA Endogenous Control. For RNA sequencing, the service was outsourced to Novogene (USA), the extracted RNA quality was evaluated with an Agilent 2100 Bioanalyzer (Agilent). A sequence library was prepared using a TruSeq Stranded mRNA kit (Illumina) and sequenced using NovaSeq 6000 (Illumina). Reads were aligned to human genome assembly hg38 and quantified using the quasi-mapper Salmon (v1.8.0). Gene-expression analysis was performed using the R Bioconductor package DESeq2 (v1.36.0). The read count matrix was normalized by size factors, and a variance stabilizing transformation (VST) was applied to the normalized expression data. The differentially expressed genes were then extracted by applying a filter of padj > 0.05 and |log2foldchange| > 1 and mapped to org.Hs.eg.db for genome wide annotation. The data was visualized using clusterProfiler (v4.4.2) and pheatmap (v1.0.12) packages.

ChIP-PCR, and ChIP-qPCR

ChIP experiments were performed using the High Sensitivity ChiP Kit (Abcam, ab185913). Briefly, organoids were fixed with PFA and whole chromatin was prepared and then sonicated to an optimal size of 300bp which was confirmed by gel electrophoresis. Chromatin was used for immunoprecipitation (IP) with either MECP2 antibody (Abcam, ab2828) or IgG1 isotype control. DNA fragments were amplified using custom primers for PCR and qPCR, and fold enrichment data were normalized to IP from IgG controls.

ChiP-reChIP

Before the first ChIP, the NR3C1 antibody (Abcam, ab24552) was crosslinked to Protein A Dynabeads (Invitrogen, 10002D). The ChIP assay was then carried out on extracts from organoids as described above. At the end of the first ChIP, DNA was eluted with elution buffer supplemented with 10 mM DTT. The eluate was then diluted in 2 volumes of wash buffer supplemented with 1x Protease Inhibitor Cocktail and 1 mM DTT. The 2nd ChIP assay was then carried out as described above.

Metabolite assays

For UGT activity assay, the HLOs and PHH were harvested and homogenized in UGT assay buffer. The enzyme activity was then analyzed using UGT activity assay (BioVision, K692) according to the manufacturer's instructions in a time course experiment. Bilirubin levels were measured by collecting the supernatant from HLOs treated with bilirubin and serum from the rats. The supernatant and serum were assayed with Bilirubin Assay Kit (Total and Direct, Colorimetric) (abcam, ab235627) and Bilirubin Assay Kit (Sigma-Aldrich, MAK126) according to the manufacturer's instructions. Albumin ELISA was carried out on the rat serum using the Human Albumin ELISA Quantitation Set (Bethyl Laboratories) according to the manufacturer's instructions. AST and ALT assays were carried out on the rat serum using the AST Activity Assay Kit (Sigma-Aldrich, MAK055) and the ALT Activity Assay Kit (Sigma-Aldrich, MAK052) according to the manufacturer's instructions. Cell viability was tested using the CellTiter-Glo® luminescent cell viability assay (Promega, G7570) and quantified by a BioTek® Synergy H1 plate reader after 72 hrs. For the functional assay of lipid transport, the HLOs were incubated with fresh media

containing 50 nM CLF (Corning, 451041) before imaging them every 30 min for 2 days. Visualization of bilirubin conjugation was achieved with 5 μM fluorescent UnaG (a kind gift from Dr. Miyawaki) which was incubated with the HLO media and imaged for 2 days (Kumagai et al., 2013).

Supplementary References

Kumagai, A., Ando, R., Miyatake, H., Greimel, P., Kobayashi, T., Hirabayashi, Y., Shimogori, T., and Miyawaki, A. (2013). A Bilirubin-Inducible Fluorescent Protein from Eel Muscle. Cell *153*, 1602-1611. 10.1016/j.cell.2013.05.038.

Okita, K., Matsumura, Y., Sato, Y., Okada, A., Morizane, A., Okamoto, S., Hong, H., Nakagawa, M., Tanabe, K., Tezuka, K.-i., et al. (2011). A more efficient method to generate integration-free human iPS cells. Nature Methods *8*, 409-412. 10.1038/nmeth.1591.

Okita, K., Yamakawa, T., Matsumura, Y., Sato, Y., Amano, N., Watanabe, A., Goshima, N., and Yamanaka, S. (2013). An efficient nonviral method to generate integration-free human-induced pluripotent stem cells from cord blood and peripheral blood cells. Stem Cells *31*, 458-466. 10.1002/stem.1293.

Pitstick, A.L., Poling, H.M., Sundaram, N., Lewis, P.L., Kechele, D.O., Sanchez, J.G., Scott, M.A., Broda, T.R., Helmrath, M.A., Wells, J.M., and Mayhew, C.N. (2022). Aggregation of cryopreserved mid-hindgut endoderm for more reliable and reproducible hPSC-derived small intestinal organoid generation. Stem Cell Reports *17*, 1889-1902. https://doi.org/10.1016/j.stemcr.2022.06.011.